Research Square

Preprints are preliminary reports that have not undergone peer review.
They should not be considered conclusive, used to inform clinical practice,
or referenced by the media as validated information.

Nonlinear Dynamic Analysis and Closed-Form Modelling of Negative Stiffness Vibration Isolation Systems under Bidirectional Excitation

K. K. Kiran
SJB Institute of Technology
Naveenkumar D. T.
naveenkumardt@sjbit.edu.in

SJB Institute of Technology

Research Article

Keywords: Nonlinear dynamics, Negative stiffness systems, Vibration isolation, Closed-form solutions, Harmonic balance method, Vibration control

Posted Date: April 16th, 2026

DOI: https://doi.org/10.21203/rs.3.rs-9355885/v1

License: This work is licensed under a Creative Commons Attribution 4.0 International License.
Read Full License

Additional Declarations: No competing interests reported.

Version of Record: A version of this preprint was published at Iranian Journal of Science and Technology, Transactions of Mechanical Engineering on June 16th, 2026. See the published version at https://doi.org/10.1007/s40997-026-00996-1.

Nonlinear Dynamic Analysis and Closed-Form Modelling of Negative Stiffness Vibration Isolation Systems under Bidirectional Excitation

K. K. Kiran[1] and Naveenkumar D. T.[2*]

[1,2] Department of Civil Engineering, SJB Institute of Technology, Bangalore, Karnataka, India
*Corresponding Author: naveendt012@gmail.com
Orcid: 0000-0001-8512-2442

Abstract

This study presents a nonlinear dynamic analysis and closed-form modelling framework for vibration isolation systems incorporating negative stiffness elements under bidirectional excitation. A two-degree-of-freedom model is formulated to capture the coupled dynamics of the primary structure and isolation mechanism, incorporating nonlinear restoring forces within a consistent analytical framework. The governing equations are developed using classical principles and subsequently simplified through Taylor series expansion and statistical linearization to obtain tractable closed-form solutions.

Unlike conventional optimization-based approaches, the proposed methodology enables direct determination of optimal system parameters, including frequency and damping ratios, without reliance on iterative procedures. The dynamic response of the system is evaluated using harmonic balance and transfer function analysis, providing insight into resonance characteristics, stability behaviour, and energy dissipation mechanisms under coupled excitations.

Comparative analyses demonstrate that the incorporation of negative stiffness significantly enhances vibration mitigation performance. The proposed closed-form solutions show good agreement with hybrid optimization methods while offering improved computational efficiency and deeper physical insight into system behaviour. The results highlight the effectiveness of negative stiffness mechanisms in modifying system dynamics and reducing response amplitudes.

The developed framework contributes to the fields of nonlinear dynamics and vibration control by providing a generalized analytical tool for the design and analysis of coupled mechanical systems with nonlinear stiffness characteristics.

Keywords: Nonlinear dynamics; Negative stiffness systems; Vibration isolation; Closed-form solutions; Harmonic balance method; Vibration control.

Statements and Declarations

Funding: The authors did not receive support from any organization for the submitted work.

Conflicts of interest/Competing interests: The authors have read the Committee on Publication Ethics guidelines and agree to abide by provisions thereof.

Availability of data and material: All the required data are generated by the authors using a software code written in MATLAB 7.0.

Author Contributions: K. K. Kiran: Conceptualization, methodology, analytical formulation, numerical modelling, writing—original draft. Naveenkumar D. T.: Supervision, validation, data interpretation, writing—review and editing, final approval of the manuscript.

Abbreviations

NNBI	Nonlinear negative stiffness isolator
TDOF	Two-degree-of-freedom
HBM	Harmonic Balance Method
NSD	Negative Stiffness Damper
DVA	Dynamic vibration absorbers
FPA	Fixed-Point Approach
MDOF	Multi-Degree-of-Freedom

Symbols

m_b	Mass of base-isolated system
k_b	Stiffness of base-isolated system
c_b	Damping of base-isolated system
k_r	Effective negative stiffness
α	Ratio of negative to conventional stiffness
m_s	Mass of single degree of freedom system
k_s	Stiffness of single degree of freedom system
c_s	Damping of single degree of freedom system
$\ddot{Z}_{gx}$	Ground accelerations along the horizontal component
$\ddot{Z}_{gy}$	Ground accelerations along the vertical component
v_{sx}	Superstructure displacements in the x axes
v_{sy}	Superstructure displacements in the y axes
v_{bx}	Isolation layer displacements along x axes
v_{by}	Isolation layer displacements along y axes
F_v	Lateral inertia force
z_{bx}	Isolator's displacement relative to the ground
L_O	Free length
L	Pre-compressed length
F_b	Isolator subjected to base excitation inside the isolator core
F_{bn}	Total nonlinear inertial force
z_{bx}	Relative displacements of the isolator in the x direction
z_{by}	Relative displacements of the isolator in the y direction
z_{sx}	Superstructure's displacement relative to the isolator along the x-axes
z_{sy}	Superstructure's displacement relative to the isolator along the y -axes
v_s	Absolute displacement of the TDOF superstructure
$z_b = Z_b e^{i\omega t}, z_s = Z_s e^{i\omega t} \& z_g = Z_g e^{i\omega t}$	Harmonic solutions, the displacements
$X_s(q)$	Response of the TDOF model
$X_b(q)$	Structural response of the NNBI

μ_b	Inerter ratio of the base isolator
ς_b	Damping ratio of the NNBI
ς_s	Damping ratio of the structural system
ω_b	Natural frequency of the isolator system
ω_s	Natural frequency of the structural system
κ	Constant
$\sigma_{z_b}^2$	Standard deviation of structural deflection
$(\omega_b)_{opt}$	Optimal frequency ratio of the NNBI
$(v_b)_{opt}$	Optimal non-dimensional form of the frequency ratio of the NNBI
$(\varsigma_b)_{opt}$	Optimal damping ratio of the NNBI
$\sigma_{z_b}^2$	The standard deviation response of NNBI
$\lvert X_s(v)\rvert$	Modulus of the transfer function
S_0- S_8	Coefficient of constant of closed form of expression

1. INTRODUCTION

The structural integrity of engineering systems particularly high-rise buildings, bridges, and offshore structures faces significant challenges due to vibrations induced by dynamic excitations such as earthquakes, waves, and wind (Wu et al. 2005). To counter these effects and improve structural resilience, numerous approaches have been explored, ranging from passive to semi-active and active devices (Colwell and Basu 2009). Among the available techniques, base isolation has gained prominence as a reliable passive attenuating seismic demands on structures (Shi et al. 2014). The core concept of base isolation lies in separating the superstructure from seismic input through specialized devices that dissipate or redirect earthquake energy, thereby reducing structural damage during intense shaking. By modifying the dynamic properties, seismic isolation ensures that the structure's natural period does not coincide with the main energy content of ground shaking or with the response frequency of a fixed-base counterpart (Jangid 2022a). The effectiveness of this technique has been well demonstrated in both new construction and retrofitting of vital infrastructure, including medical, firefighting, and emergency response facilities (De Luca and Guidi 2019). By minimizing the transmission of seismic forces to the superstructure, base isolation not only reduces structural damage but also protects nonstructural components and building contents (Jangid 2022b). This, in turn, enhances the overall performance of the structure and ensures occupant safety during major seismic events (Jangid 2023). Moreover, this technique is instrumental in ensuring the safety of critical infrastructure, including power plants and emergency response centers (Lyu et al. 2025; Panchal and Jangid 2012). In addition, recent studies on vibration control in nonlinear mechanical systems have demonstrated the effectiveness of advanced analytical and control strategies for mitigating dynamic responses (Efafi et al. 2022).

In recent years, numerous configurations of Negative Stiffness Damper NSDs have been introduced and investigated for diverse structural applications (Tang et al. 2025). The primary function of NSDs is to lower the effective system stiffness while maintaining its load-bearing ability in directions perpendicular to the excitation (Hu and Zhou 2025). Mechanically, an NSD generates a restoring force opposite in direction to that of conventional elastic materials (Pasala et al. 2013). This distinctive characteristic allows NSDs to attenuate unwanted vibrations in systems exposed to dynamic actions including seismic events, aerodynamic forces, and hydrodynamic effects (Hewage et al. 2016). Moreover, negative stiffness dampers can dissipate seismic energy

and reduce the transmission of inertial forces to the superstructure, thereby limiting structural and nonstructural damage (Islam and Jangid 2023). Recent developments in vibration isolation systems with adjustable high static–low dynamic stiffness characteristics further highlight the potential of negative stiffness mechanisms in enhancing vibration attenuation performance (Su et al. 2022c). Although several benefits of NSDs have been identified, the development of closed-form formulations for systems with nonlinear negative stiffness under bidirectional seismic loading has not been thoroughly investigated. To fill this gap, this work establishes exact analytical expressions for structures isolated at the base and equipped with nonlinear negative stiffness dampers.

The mechanical parameters play a crucial role in defining the performance of dynamic vibration absorbers (DVAs). A thorough understanding of these parameters is essential for optimizing DVA design, where optimization techniques become indispensable. Traditionally, the H_2 and H_∞ optimization methods are the most widely employed approaches for determining the optimal parameters of DVAs (Asami et al. 2002; Asami and Nishihara 1999, 2002; Cheung and Wong 2011; Ormondroyd and Den Hartog 2023). The H_∞ method is based on minimizing the maximum amplitude of the transfer function, typically corresponding to the peak structural response under harmonic excitation. The Fixed-Point Approach (FPA) (Den Hartog 1947) also provides algebraic expressions and closed-form solutions for optimal parameters and is closely associated with the H_∞ optimization method (Ikago et al. 2012; Shen et al. 2017; Su et al. 2022a; Xiaoran et al. 2016). In more complex scenarios, the H_∞ method continues to be a useful tool for parameter identification (Garrido et al. 2013; Hu and Chen 2015; Kapasakalis et al. 2020; Su et al. 2022b; Xu et al. 2022). In contrast, the H_2 method is effective under white noise excitation, relying on frequency-domain integration of the transfer function to obtain optimal values (Di Matteo et al. 2019; Kiran et al. 2024; Su et al. 2023). However, both H_2 and H_∞ approaches often neglect higher-order data fitting, limiting their accuracy in deriving empirical formulas for optimal parameters. To overcome these limitations, have been developed, which incorporate filter coefficients to improve parameter estimation (Su et al. 2024a). In addition, stability maximization criteria have been used to determine optimal parameters for structures subjected to harmonic excitation (Kiran et al. 2023).

Beyond these traditional approaches, nonlinear vibration absorbers have been proposed to mitigate structural response through reliability-based design frameworks (Kiran et al. 2025; Liu et al. 2024). Recent developments include innovative configurations such as the magnetically tuned tetrahedral system with nonlinear inertia, which utilizes nonlinear methods together with the HBM to attenuate seismic vibrations (Yan et al. 2023). And the Scotch Yoke Inerter, designed to reduce seismic vibrations effectively (Zhang et al. 2023). Several studies have investigated nonlinear isolation systems for vibration mitigation (Niu et al. 2024), with extensive research dedicated to nonlinear analysis of structural responses under dynamic loads (Akbari et al. 2025; Li et al. 2025; Roy-Layinde et al. 2025; Zhang et al. 2025). A few researchers have also examined structural performance under horizontal bidirectional seismic excitations (Al-Fahdawi and Barroso 2021; Hosseinzadeh and Galal 2021).

Recent studies have explored advanced isolation strategies such as negative stiffness–inerter combinations (Islam and Jangid 2023), H_2-optimal tuned mass dampers with negative stiffness and inerters under bidirectional loading (Kiran et al. 2024), and hybrid damping systems integrating negative stiffness devices with optimization techniques (Kiran et al. 2023). While these works have demonstrated the potential of nonlinear isolators, they primarily rely on numerical formulations, hybrid optimization schemes, or unidirectional excitation models, and therefore do not provide concise analytical solutions suitable for practical design. Some of the researchers are investigated on mitigations of seismic excitation of structure with different dampers (Rong et al. 2025; Zhu et al.

2025). As far as can be determined from the available literature, closed-form expressions for *Nonlinear Negative Stiffness Base Isolators (NNBIs) under bidirectional seismic excitation have not yet been reported.*

To address this gap, the present study makes the following contributions: (i) develops *exact closed-form solutions* for base-isolated structures with nonlinear negative stiffness isolators under bidirectional seismic excitations using Taylor series expansion and analytical methods; (ii) introduces a *concise analytical solution framework* that enables direct determination of optimal design parameters without iterative optimization; (iii) evaluates the seismic response mitigation effectiveness of NNBIs through transfer function and harmonic balance methods; (iv) compares the proposed concise analytical solutions with hybrid optimization and existing methods, demonstrating their *superiority in accuracy and transparency*; and (v) to validate the proposed analytical solutions against results from previous research on NNBIs.

From a mechanics perspective, the present study contributes to the analytical understanding of nonlinear dynamical systems incorporating negative stiffness characteristics under coupled excitations. The formulation establishes a direct relationship between system parameters and dynamic response through closed-form expressions, thereby providing insight into the role of nonlinear stiffness in modifying resonance behaviour, energy transfer mechanisms, and stability properties. The proposed framework extends classical vibration theory by integrating nonlinear restoring forces with bidirectional coupling effects, offering a generalized analytical approach applicable to a broader class of coupled mechanical systems beyond specific engineering applications.

2. STRUCTURE MODEL AND EQUATION OF MOTION

A TDOF system isolated with NNBI under bidirectional seismic excitation is illustrated in Fig 1. Here, m_b, k_b and c_b denote respectively the damper's mass, stiffness, and damping characteristics within the base the base-isolated system. The effective negative stiffness is represented by k_r, defined as $k_r = \alpha k_b$, where α is the ratio of negative to conventional stiffness. For the TDOF superstructure, m_s, k_s and c_s correspond to its mass, stiffness, and damping parameters. The seismic inputs are modelled as ground accelerations, $\ddot{Z}_{gx}$ denoting the horizontal component and $\ddot{Z}_{gy}$ the vertical component. The superstructure displacements in the x- and y-axes are represented by v_{sx} and v_{sy}. Similarly, the isolation layer displacements along same axes are indicated by v_{bx}&v_{by}. The nonlinear negative stiffness damper plays a significant role in mitigating the bidirectional seismic response of structural systems. It is effective under both near-fault and far-field ground motion excitations, including pulse-type motions. Therefore, the nonlinear negative stiffness damper is considered as a passive vibration control device in the present study. The structural system is subjected to simultaneous ground motions in both horizontal and vertical directions.

The nonlinear negative stiffness device provides an extended isolation period, thereby reducing the shear deformation of the isolation layer in systems subjected to strong ground motions, including near-field earthquakes. Since the device operates without the need for external power, it is considered a *passive control system*. In the present investigation, a model similar to that of a base-isolated structure equipped with different control devices, as examined in previous studies, is considered. However, unlike earlier work, the present study incorporates concise analytical solutions, which were not addressed previously. The NNBI operates based on a friction-related parameter that significantly influences its nonlinear behavior. The lateral inertia force, which develops due to the horizontal seismic excitations, can be expressed as

$$F_v = k_r z_{bx}\left(1 - \frac{L_O}{\sqrt{z_{bx}^2+L^2}}\right) + k_r z_{by}\left(1 - \frac{2L_O}{\sqrt{z_{by}^2+L^2}}\right) \quad (1)$$

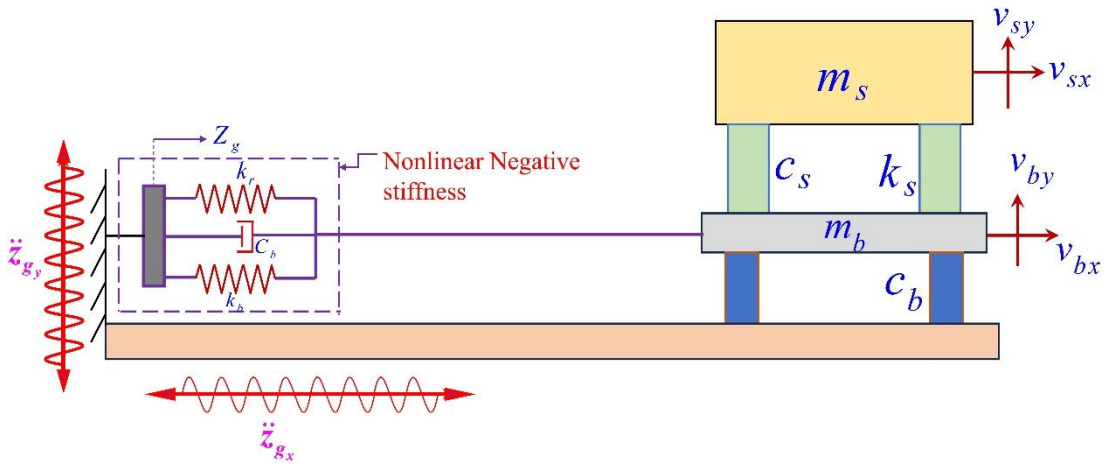


Fig. 1. TDOF system with NNBI under bidirectional seismic excitations.

Where $z_{bx} = v_{bx} - z_g$ denotes the isolator's displacement relative to the ground. Fig. 1 depicts the TDOF configuration equipped with a nonlinear negative stiffness element together with the isolator, placed in parallel. In this schematic, L_O and L correspond to the free length and the pre-compressed length, respectively. Carrella et al., (2009) proposed a compromise technique using Taylor series expansion to approximate nonlinear expressions and obtain solutions for systems with nonlinear components through harmonic methods. In the present study, this concept is extended to develop *concise analytical solutions* in conjunction with hybrid optimization techniques. Furthermore, Eq. (2) provides a simplified expression of the nonlinear restoring force.

The analysis is carried out under these simplifying assumptions: (i) the system is idealized as a TDOF model, (ii) Multi-Degree-of-Freedom (MDOF) influences are disregarded, and (iii) soil–structure interaction effects are excluded. With these considerations, the nonlinear restoring force of the isolator along the x- and y-axes is formulated as

$$F_{vn} = \left[-k_r\left(\frac{L_O}{L}\right)z_{bx} - k_r z_{bx}^2 + \left(\frac{L_O}{2L^3}\right)k_r z_{bx}^3\right] + \left[-k_r\left(\frac{L_O}{L}\right)z_{by} - k_r z_{by}^2 + \left(\frac{L_O}{2L^3}\right)k_r z_{by}^3\right] \quad (2)$$

For the isolator subjected to base excitation inside the isolator core, the inertial force is given by

$$F_b = \left[k_b z_{bx} + 2k_b z_{by}\right] \quad (3)$$

Since both springs act in parallel, the *total nonlinear inertial force* arrived of the NNBI system is obtained as

$$F_{bn} = F_{vn} + F_b \quad (4)$$

Using Newton's second law, the governing dynamics of the TDOF system are formulated. Consequently, the isolator's motion equations take the form

$$\begin{aligned} &m_b\ddot{v}_{bx} + c_b\left(\dot{v}_{bx} - \dot{z}_g\right) = -F_{bn} + k_s(v_s - v_b) + c_s(\dot{v}_s - \dot{v}_b) \\ &m_b\ddot{z}_{bx} + c_b\dot{z}_{bx} + k_b z_{bx} - k_r\left(\frac{2L_O}{L}\right)(z_{bx} + z_{by}) - k_r(z_{bx} + z_{by}) \\ &+ \left(\frac{3L_O}{2L^3}\right)k_r(z_{bx}^3 + z_{by}^3) - c_s\dot{z}_s - k_s(z_{sx} + z_{sy}) = -m_b\ddot{z}_g \end{aligned} \quad (5)$$

Where $z_{bx} = [v_{bx} - z_g]$ and $z_{by} = [v_{by} - z_g]$ represent the relative displacements of the isolator in the x- and y-directions with respect to the ground. Similarly, $z_{sx} = [v_{sx} - v_{bx}]$ & $z_{sy} = [v_{sy} - v_{by}]$ define the

superstructure's displacement relative to the isolator along the x- and y-axes. The governing equations of motion of the superstructure mass are given by

$$m_s\ddot{v}_s + c_s(\dot{v}_s - \dot{v}_b) - k_s(v_s - v_b) = 0$$
$$m_s\left(\ddot{z}_s + \ddot{z}_b + \ddot{z}_g\right) + c_s\dot{z}_s + k_s z_s = 0 \quad (6)$$

Here, the absolute displacement of the TDOF superstructure is given by

$$v_s = \left(z_{sx} + z_{sy} + z_{bx} + z_{by} + z_g\right)$$

Combining Eqs. (5) and (6) yields the governing dynamic equation for the TDOF base-isolated system incorporating nonlinear negative-stiffness isolators under bidirectional seismic loading.

$$m_b\left(\ddot{z}_b + \ddot{z}_g\right) + c_b\dot{z}_b + (k_b - k_r)z_b - k_r\left(\frac{2L_0}{L}\right)z_b + \left(\frac{3L_0}{2L^3}\right)k_r z_b^3 - c_s\dot{z}_s - k_s z_s = 0$$
$$m_s\left(\ddot{z}_s + \ddot{z}_b + \ddot{z}_g\right) + c_s\dot{z}_s + k_s z_s = 0 \quad (7)$$

A *statistical linearization approach* is utilized to derive approximate solutions for the nonlinear governing equations, whereas an *analytical optimization* method is adopted to identify the optimal system parameters. From Eq. (7), the statistical linearization method (Chowdhury and Banerjee 2023) is adopted in conjunction with both *hybrid* and *concise analytical solution approaches*. Validation of these methods is performed by evaluating their accuracy through *time-domain analyses*.

Prior studies highlight statistical linearization as a well-recognized approach, especially suitable for systems excited by Gaussian white noise processes with zero mean. In contrast, the *Taylor series expansion* is employed in the present study to derive concise analytical solutions, as it enables the nonlinear terms to be represented in simplified algebraic form, thereby avoiding higher-order differential formulations and yielding more precise closed-form expressions.

Accordingly, *two distinct closed-form solutions* are derived using the proposed optimization techniques applied to the isolator system. From Eq. (7), the nonlinear restoring element is systematically linearized, and simplified expressions are obtained for practical implementation.

$$k_r^e = E\left\{\frac{\partial\left(\left(\frac{3L_0}{2L^3}\right)k_r z_b^3\right)}{\partial z_b}\right\} = 3\sigma_{z_b}^2\left(\frac{3L_0}{2L^3}\right)k_r \quad (8)$$

Eq. (8) is substitute into Eq. (7) and revised governing equation of motion has arrived as

$$m_b\left(\ddot{z}_b + \ddot{z}_g\right) + c_b\dot{z}_b + k_b z_b - k_r\left(\frac{L_O}{L} + 2\right)z_b + 5\sigma_{z_b}^2\left(\frac{L_O}{2L^3}\right)k_r z_b - (c_s\dot{z}_s - k_s z_s) = 0$$
$$m_s\left(\ddot{z}_s + \ddot{z}_b + \ddot{z}_g\right) + 2c_s\dot{z}_s + k_s z_s = 0 \quad (9)$$

In the first step, from Eq. (9), the variance is assumed to be zero, i.e., $\sigma_{z_b}^2 = 0$, to derive an exact closed-form solution when the system is subjected to stochastic white noise input. This simplification also facilitates the application of the hybrid optimization technique. Subsequently, by employing both the hybrid optimization approach and concise analytical solutions, the optimal parameters of the system are determined. The revised dynamic equations of the system can therefore be written in the form

$$(m_b\ddot{z}_b + c_b\dot{z}_b + k_b z_b) - (\kappa k_r z_b) - (c_s\dot{z}_s + k_s z_s) = -m_b\ddot{z}_g$$
$$m_s\left(\ddot{z}_s + \ddot{z}_b + \ddot{z}_g\right) + c_s\dot{z}_s + k_s z_s = 0 \quad (10)$$

Here, $\kappa = \left(\frac{2L_O}{L} + 1\right)$.

Assuming time-invariant harmonic solutions, the displacements are expressed as $z_b = Z_b e^{i\omega t}, z_s = Z_s e^{i\omega t} \& z_g = Z_g e^{i\omega t}$. By substituting these terms into Eq. (10), the system's transfer function can be expressed in the form of

$$\begin{bmatrix} ((-\kappa\alpha + 1)\omega_b^2 + 4q\varsigma_b\omega_b + q^2)\mu_b & -4\varsigma_s\omega_s q - \omega_s^2 \\ q^2 & 2\varsigma_s\omega_s q + 2\omega_s^2 \end{bmatrix} \begin{Bmatrix} Z_b \\ Z_s \end{Bmatrix} = -\begin{bmatrix} \mu_b \\ 1 \end{bmatrix} Z_g \tag{11}$$

To obtain the vibration characteristics of the decoupled structure, the transfer function method is applied together with hybrid and simplified analytical techniques. Closed-form relations are then derived through various optimization strategies, allowing precise assessment of the vibrational behaviour for the base-isolated configuration.

The response of the TDOF model can be represented by

$$X_s(q) = \left(\frac{Z_s}{Z_g}\right) = \frac{\mu_b\omega_b^2 - 2\alpha\kappa\mu_b\omega_b^2 + 4\mu_b\varsigma_b\omega_b q}{\delta} \tag{12}$$

Correspondingly, the structural response of the NNBI formulation may be written as

$$X_b(q) = \left(\frac{Z_b}{Z_g}\right) = \frac{2\mu_b q\omega_s + 2\mu_b q^2 + \mu_b\omega_s^2 + 4\varsigma_s\omega_s q + \omega_s^2}{\delta} \tag{13}$$

The common denominator in Eqs. (12) and (13) is expressed as

$$\begin{aligned} \delta = {} & \mu_b q^4 + (4\mu_b\varsigma_b\omega_b + 4\mu_b\varsigma_s\omega_s)q^3 + (-\alpha\kappa\mu_b\omega_b^2 + 4\mu_b\varsigma_b\varsigma_s\omega_s\omega_b + 2\mu_b\omega_b^2 + \mu_b\omega_s^2 + \omega_s^2)q^2 \\ & + (-2\alpha\kappa\mu_b\omega_b^2\varsigma_s\omega_s + 4\mu_b\varsigma_b\omega_b^2\omega_s^2 + 4\mu_b\varsigma_s\omega_b^2\omega_s^2 - \mu_b\alpha\kappa\mu_b\omega_b^2\omega_s^2 + 4\mu_b\varsigma_s\omega_b^2\omega_s)q \\ & - \alpha\kappa\mu_b\omega_b^2\omega_s^2 + 2\mu_b\omega_b^2\omega_s^2 \end{aligned} \tag{14}$$

3. ANALYTICAL OPTIMIZATION TECHNIQUE

For identifying the optimal configuration of the NNBI, a pair of complementary design refinement methods are employed: the Hybrid Optimization Technique and the Concise Analytical Solution Method. These methods are utilized to extract essential parameters like the damping ratio along with the frequency ratio directly from the system equations.

In this research, vibration behavior of the isolator is evaluated by considering the standard deviation of structural deflection (i. e. $\sigma_{z_b}^2 \neq 0$). The presence of a non-zero displacement variance is essential for accurately characterizing the stochastic vibration of the system under seismic loading. By substituting $\sigma_{z_b}^2 \neq 0$ into Eq. (10), explicit analytical solutions corresponding to the base-isolation system are obtained.

The following subsections present the two optimization techniques in detail:

3.1 Hybrid Optimization

An integrated optimization method is applied for identifying ideal parameters for the base-isolated system under random excitation. This method evaluates the structural response across all frequencies while minimizing the total energy of the system. Unlike traditional optimization schemes, the hybrid approach is versatile, being applicable to both Gaussian type white noise and harmonic excitation.

For the purposes of this research, the excitation is characterized using a zero-mean Gaussian white noise characterized by a variance of two. For analytical tractability, Eq. (12) is considered with $\varsigma_s = 0$, and the response standard deviation is optimized with the help of the hybrid optimization technique. This procedure yields an explicit polynomial formulation of the system behavior, given by

$$\begin{aligned} \delta = {} & 2\mu_b q^4 + 4\mu_b q^3\varsigma_b\omega_b + (\mu_b\omega_b^2 - \alpha\kappa\mu_b\omega_b^2 + \mu_b\omega_s^2 + 2\omega_s^2)q^2 \\ & + 4\mu_b q\varsigma_b\omega_b\omega_s^2 - \alpha\kappa\mu_b\omega_b^2\omega_s^2 + \mu_b\omega_b^2\omega_s^2 \end{aligned} \tag{15}$$

From Eq. (15), the fourth-order polynomial expression leads to the vibration response variance of the TDOF model, expressed in the form:

$$\sigma_{z_s}^2 = \frac{S_0\pi\omega_b\left(\mu_b(\alpha\kappa-1)^4\omega_b^4-\omega_s^4\left(-4\mu_b\varsigma_b^2+\alpha\kappa-1\right)\right)}{2\varsigma_b\omega_s^8} \tag{16}$$

To obtain the optimal parameters, Eq. (16) is differentiated as follow to yield

$$\frac{\partial\sigma_{z_s}^2}{\partial\varsigma_b} = 0 \text{ and } \frac{\partial\sigma_{z_s}^2}{\partial\omega_b} = 0 \tag{17}$$

By substituting Eq. (16) into the first expression of Eq. (17), the damping ratio of the NNBI is obtained as

$$\varsigma_b = \frac{\sqrt{\mu_b\left(\alpha^2\kappa^2\mu_b\omega_b^2-4\alpha\kappa\mu_b\omega_b^2-\alpha\kappa\omega_s^2+2\mu_b\omega_b^2+\omega_s^2\right)}}{4\mu_b\omega_s} \tag{18}$$

Next, substituting Eq. (18) into Eq. (16) yields an improved expression for the variance of the TDOF vibrational response

$$\sigma_{x_s}^2 = \frac{2\mu_b S_0\pi\omega_b(\alpha\kappa-1)\left(\omega_b^4(\alpha\kappa-1)\mu_b-\omega_s^2\right)}{\sqrt{\mu_b\left(\omega_b^2(\alpha\kappa-1)\mu_b-\omega_s^4\right)(\alpha\kappa-1)\omega_s^5}} \tag{19}$$

Substituting Eq. (19) into the second expression of Eq. (17), the optimal frequency ratio is obtained in closed form as:

$$(\omega_b)_{opt} = \frac{\pi S_0 S_1\omega_s}{\left(\sqrt{4\mu_b-4\mu_b\kappa\alpha^2}\right)S_2} \tag{20}$$

The dimensionless form of Eq. (20) can be written in the form

$$(\nu_b)_{opt} = \frac{1}{\sqrt{4\mu_b-4\mu_b\kappa\alpha}} \tag{21}$$

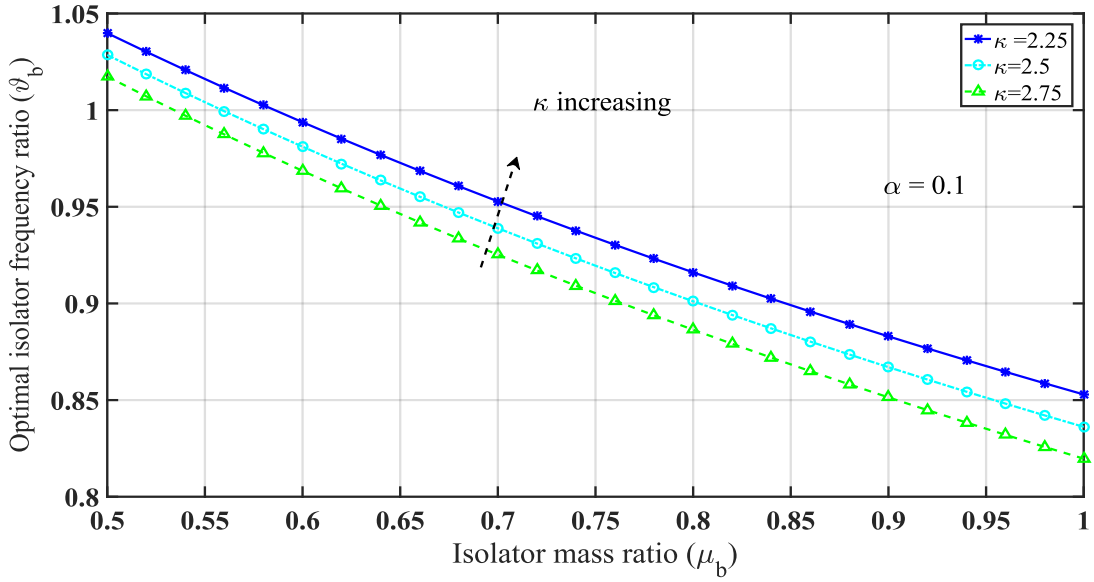
By substituting Eq. (20) into Eq. (18), the exact closed-form expression of the optimal damping ratio of the NNBI is obtained as:

$$(\varsigma_b)_{opt} = \frac{S_3}{S_4} \tag{22}$$

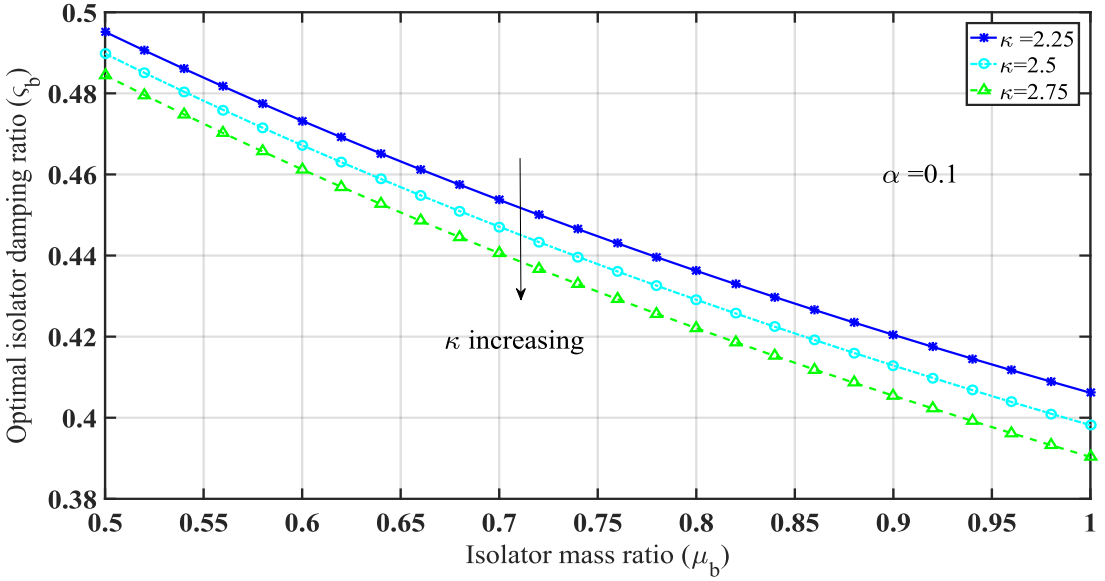
Finally, the system response of the NNBI, expressed through the standard deviation, takes the form

$$\sigma_{z_b}^2 = \frac{S_0\pi\left(-\mu_b\omega_s^2+\left(-2\omega_s^2+4\omega_b^2(\alpha\kappa-1)\right)\mu_b-2\omega_s^2\right)}{4\mu_b^2\varsigma_b\omega_b^2\omega_s^2(\alpha\kappa-1)} \tag{23}$$

Fig. 2(a) illustrates the variation of the optimal frequency ratio of the NNBI with respect to the isolator mass ratio for different values of the length ratio. It is observed that as the isolator mass ratio increases, the optimal frequency ratio decreases, while an increase in length ratio leads to higher optimal frequency ratios. The behaviour of the tuned damping ratio is shown in Fig. 2(b) indicating that the mass-to-spring and length-to-spring ratios play a significant role in the NIMBI'S damping performance.



(a)



(b)

Fig. 2. Optimum parameters vs. mass ratio for different length ratios (Hybrid Optimization).

3.2 Concise Analytical Solutions

The concise analytical solution method is employed to derive the non-dimensional dynamic response of the structural system. For this purpose, the steady-state harmonic responses are assumed in the form:

$z_b = Z_b e^{i\omega t}, z_s = Z_s e^{i\omega t} \& z_g = Z_g e^{i\omega t}$

Substituting these expressions into Eq. (10), the governing transfer function can be written as:

$$\begin{bmatrix} A_{11} & -4i\varsigma_s\nu - 2 \\ -\nu^2 & -2\nu^2 + 4i\varsigma_s\nu + 2 \end{bmatrix} \begin{Bmatrix} Z_b \\ Z_s \end{Bmatrix} = -\begin{bmatrix} \mu_b \\ 2 \end{bmatrix} \frac{Z_g}{\omega_s^2}$$

$$A_{11} = -\mu_b\nu^2 + 4i\mu_b\varsigma_b\nu_b\nu - 2\mu_b\nu_b^2\alpha\kappa + \alpha\mu_b\nu_b^2 \quad (24)$$

The vibration response of the TDOF model is given by

$$X_s(\nu) = \left(\frac{Z_s}{Z_g}\right)\omega_s^2 = \frac{-4i\mu_b\nu\varsigma_s - 4i\varsigma_s\nu + 2\mu_b\nu^2 - \mu_b - 1}{\delta} \quad (25)$$

Similarly, the vibration response of the NNBI is expressed as

$$X_b(\nu) = \left(\frac{Z_b}{Z_g}\right)\omega_s^2 = \frac{-4i\mu_b\nu\varsigma_s - 4i\varsigma_s\nu + 2\mu_b\nu^2 - \mu_b - 1}{\delta} \tag{26}$$

The common denominator of Eqs. (25) and (26) is given by:

$$\delta = \alpha\kappa\mu_b\nu^2\nu_b^2 - 6\mu_b\nu^2\nu_b^2\varsigma_b\varsigma_s - 2\mu_b\nu_b^2\alpha\kappa + \mu_b\nu^4 - \mu_b\nu^2\nu_b^2 - \mu_b\nu^2 + 6\mu_b\nu_b^2 - \nu^2 + i(-2\alpha\kappa\mu_b\nu_b^2\nu\varsigma_s - 4\mu_b\nu^3\nu_b\varsigma_b - 2\mu_b\nu^3\varsigma_s + 2\mu_b\nu_b^2\nu\varsigma_s + 4\mu_b\nu_b\nu\varsigma_b - 2\nu^3\varsigma_s) \tag{27}$$

It can be seen that the peak vibrational behaviour of the isolated TDOF system is greatly reduced by applying the concise analytical solution for the NNBI. To identify the ideal natural frequency together with the corresponding damping coefficient, the modulus of the transfer function is considered as

$$|X_s(\nu)| = \sqrt{\frac{X_1^2 + \varsigma_b^2 X_2^2}{X_3^2 + \varsigma_b^2 X_4^2}} = \left|\frac{X_2}{X_4}\right| \sqrt{\frac{\left(\frac{X_1}{X_2}\right)^2 + \varsigma_b^2}{\left(\frac{X_3}{X_4}\right)^2 + \varsigma_b^2}} \tag{28}$$

Where

$$X_1 = -\kappa\alpha\mu_b\nu_b^2 + 2\mu_b\nu_b^2$$
$$X_2 = 4\mu_b\nu_b\nu$$
$$X_3 = \kappa\alpha\mu_b\nu_b^4\nu^4 - \kappa\alpha\mu_b\nu_b^2 + \mu_b\nu^6 - \mu_b\nu_b^4\nu^4 - \mu_b\nu^2 + \mu_b\nu_b^2 - \nu^2 \tag{29}$$

Based on Eq. (28), couple of distinct conditions are obtained to determine the ratio of natural frequency pertaining to NNBI (Bishop 1957; Chowdhury and Banerjee 2023). These are expressed as:

$$\left|\left(\frac{X_1}{X_2}\right)^2\right|_{\nu_j} = \left|\left(\frac{X_3}{X_4}\right)^2\right|_{\nu_j} \text{ and } \left|\left(\frac{X_1}{X_2}\right)^2\right|_{\nu_1} = \left|\left(\frac{X_3}{X_4}\right)^2\right|_{\nu_2} \tag{30}$$

By substituting the 1st condition of Eq. (30), the following governing expression is obtained (Chowdhury et al. 2022):

$$\mu_b\nu^6 + (2\kappa\alpha\mu_b\nu_b^2 - 2\mu_b\nu_b^4 - \mu_b - 1)\nu^2 - 2\kappa\alpha\mu_b\nu_b^2 + 2\mu_b\nu_b^2 = 0 \tag{31}$$

Rearranging Eq. (31), the relation can be written as

$$\nu^6 + (-\nu_1^4 - \nu_2^4)\nu^2 + \nu_1^2\nu_2^2 = 0 \tag{32}$$

From the comparison of Eqs. (31) and (32), the combined value of the roots can be written as

$$\nu_1^4 + \nu_2^4 = -4\kappa\alpha\nu_b^2 + 4\nu_b^2 + 1 + \mu_b^{-1} \tag{33}$$

Again from Eq. (30), using the 2nd condition, the sum of the roots is alternatively obtained in the form

$$\nu_1^4 + \nu_2^4 = 4 \tag{34}$$

Equating Eq. (33) and Eq. (34), the ratio of ideal natural frequency of the NNBI is expressed in the form

$$(\nu_b)_{opt} = \sqrt{\frac{S_5(1-\mu_6)}{S_6(4\mu_b - 4\kappa\alpha\mu_b)}} \tag{35}$$

From Eqs. (31), (32), (34), and (35), the optimal roots $(\nu_1)^2_{opt}$ and $(\nu_2)^2_{opt}$ are obtained. Hence, the explicit solution corresponding to the optimum roots is given by

$$\left(\nu_{1,2}\right)^2_{opt} = \frac{2 \pm \sqrt{\mu_b^2 - \mu_b + 1}}{2\mu_b} \tag{36}$$

From Eqs. (28) and (36), the ratio of optimum damping corresponding to NNBI is arrived. The resulting mathematical expression is given as:

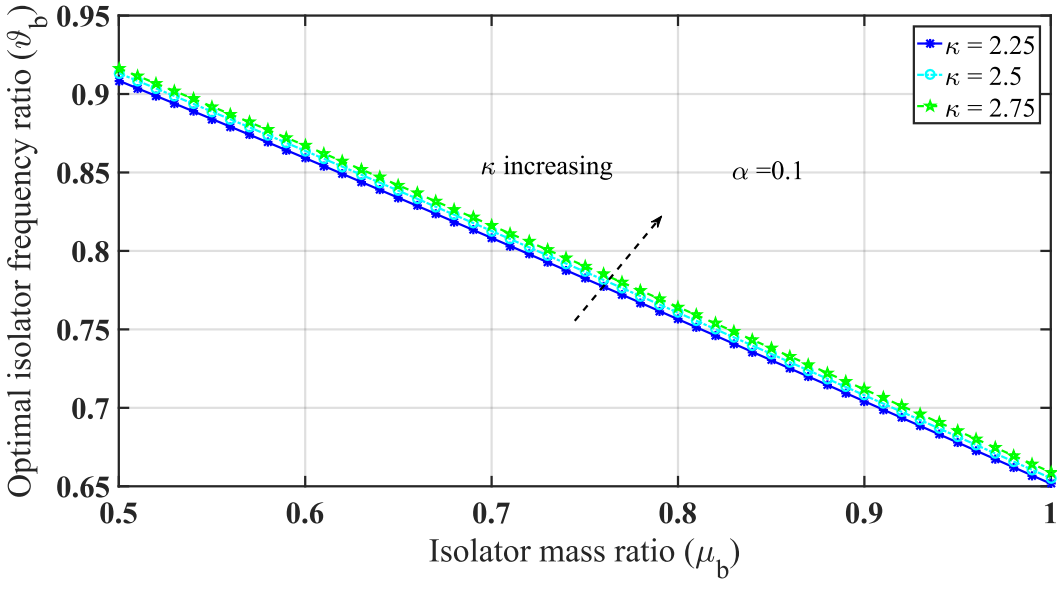
$$(\varsigma_b)_{opt} = \sqrt{\frac{S_7}{S_8}} \tag{37}$$

The governing quartic equation associated with the damping ratio can be expressed as:

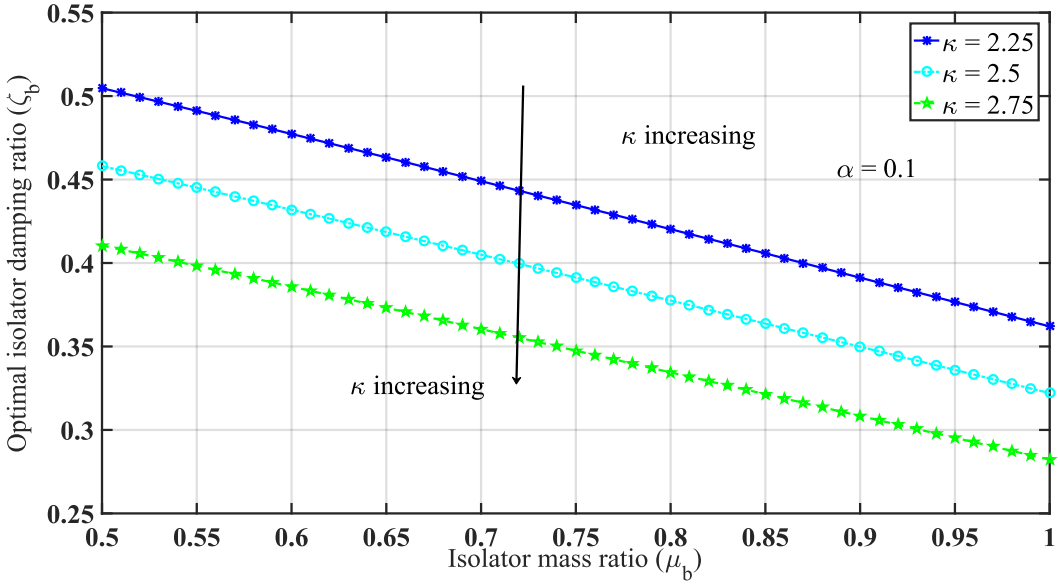
$$\begin{aligned}&(-64\mu_b^3 + 256\mu_b^2 - 350\mu_b + 256)\varsigma_b^4 + \begin{pmatrix}-48\mu_b^3\alpha\kappa + 144\mu_b^2\alpha\kappa - 160\alpha\kappa\mu_b + 48\mu_b^3 \\ +96\alpha\kappa - 144\mu_b^2 + 160\mu_b - 96\end{pmatrix}\varsigma_b^2 \\ &+5\mu_b^3\alpha^2\kappa^2 - 22\mu_b^2\alpha^2\kappa^2 + 22\mu_b\alpha^2\kappa^2 - 10\mu_b^3\alpha\kappa - 5\alpha^2\kappa^2 + 22\alpha\kappa\mu_b^2 - 22\alpha\kappa\mu_b + 5\mu_b^3 \\ &+20\alpha\kappa - 22\mu_b^2 + 22\mu_b - 25 = 0\end{aligned} \tag{38}$$

From Eq. (38), the explicit solution corresponding to the optimum damping ratio of the NNBI is expressed as

$$(\varsigma_b)^2_{opt} = \frac{\begin{matrix}68\mu_b^3\alpha\kappa - 244\mu_b^2\alpha\kappa + 160\alpha\kappa\mu_b - 48\mu_b^3 \\ -128\alpha\kappa + 244\mu_b^2 - 220\mu_b + 108\end{matrix} + \sqrt{384\begin{pmatrix}22\mu_b^6 - 108\mu_b^5 + 321\mu_b^4 - 420\mu_b^3 \\ +329\mu_b^2 - 192\mu_b + 56\end{pmatrix}(\alpha\kappa - 1)^2}}{545 - 196\mu_b^3 + 524\mu_b^2 - 684\mu_b} \tag{39}$$



(a)

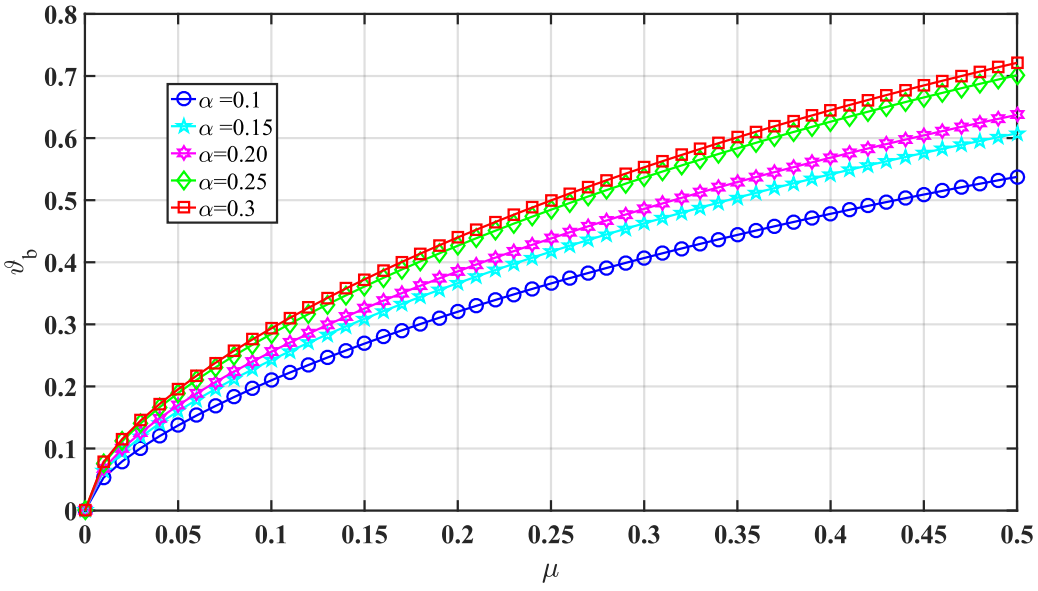


(b)

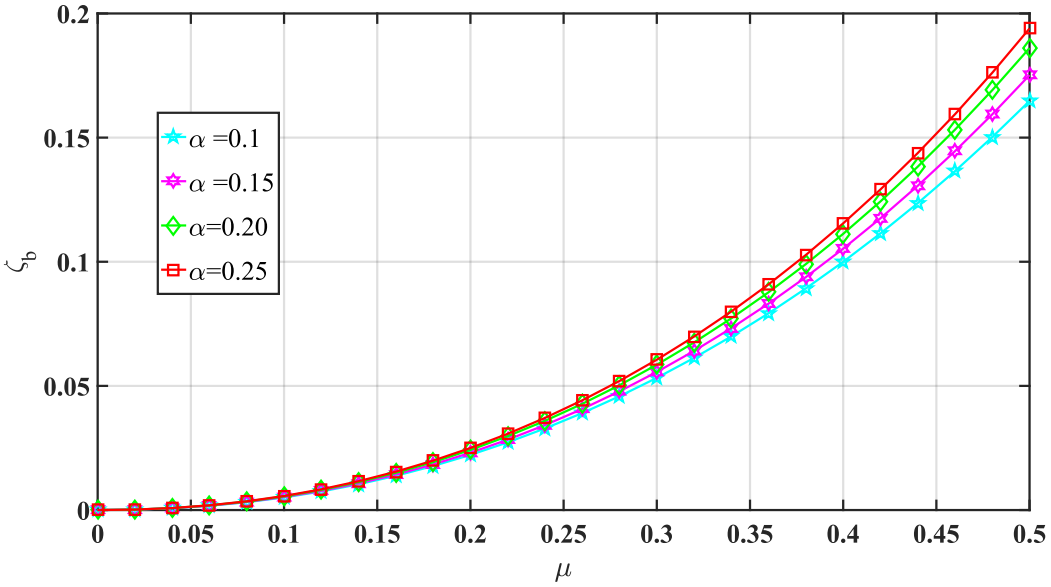
Fig. 3. Optimum parameters vs. mass ratio for different length ratios (Concise Analytical Solutions).

Figure 3(a) depicts the dependence of the frequency ratio on isolator mass ratio for varying length ratios. A higher mass ratio corresponds to lower frequency ratios, whereas larger length ratios cause them to rise. As shown in Fig. 3(b), damping ratio exhibits an inverse relation with isolator mass ratio but grows with higher length ratios. For the range of length ratios considered (2.25-2.75), both damping ratio and frequency ratio display curvilinear variation, consistent with the concise analytical method.

Fig. 4(a) presents the change in mass ratio against the optimal isolator frequency ratio for different length ratios (0.1, 0.15, 0.2 and 0.25) of the NNBI under bidirectional seismic excitation using the hybrid optimization technique. Similarly, Fig. 4(b) depicts the variation of the mass ratio against the optimal isolator damping ratio for the same set of length ratios. It is observed that, under the concise analytical solution, the optimum damping ratio exhibits different variation trends compared with the hybrid approach.



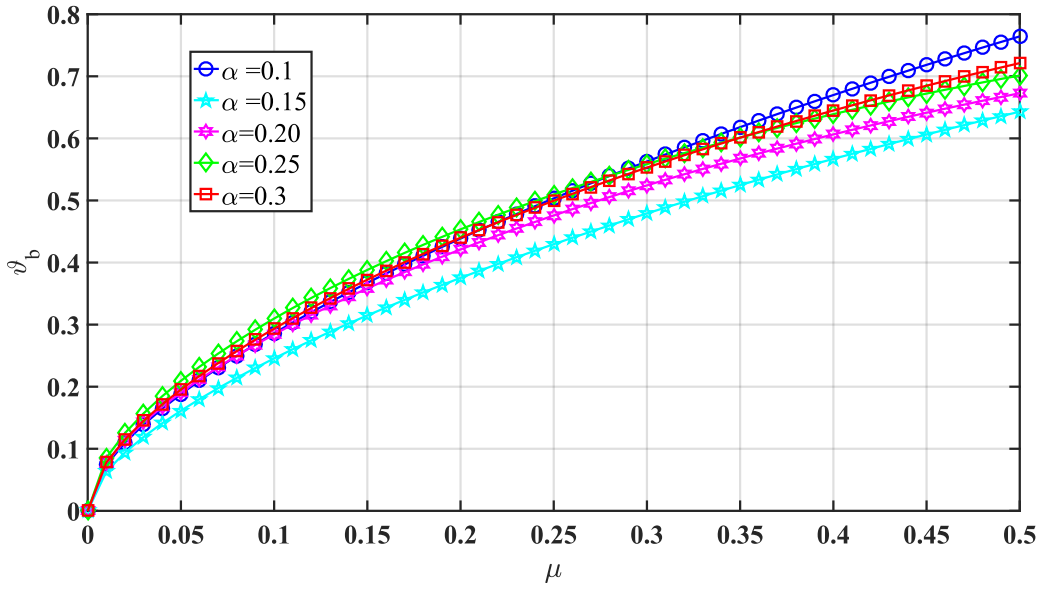
(a)



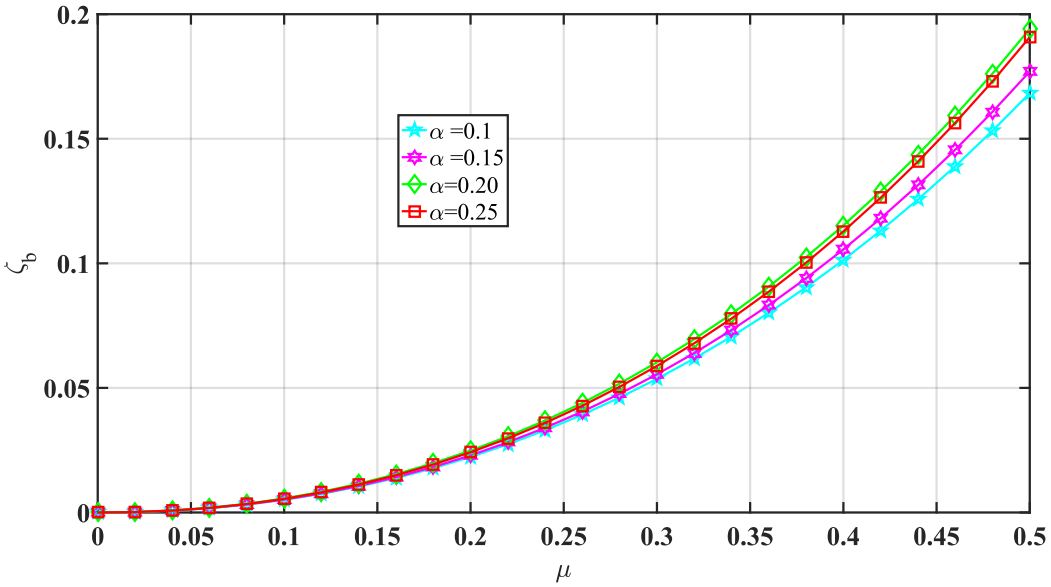
(b)

Fig. 4. Optimum parameters vs. mass ratio for varying length ratios (Hybrid Optimization).

Fig. 5(a) illustrates the change in the mass ratio against the optimal isolator frequency ratio for different negative stiffness ratios (0.1, 0.15, 0.2 and 0.25) of the NNBI under bidirectional seismic excitation, again based on the hybrid optimization technique. Fig. 5(b) illustrates the corresponding variation of the mass ratio against the optimal isolator damping ratio for the same negative stiffness ratios. Here also, the concise analytical solution produces distinct variation patterns in the optimum damping ratio compared to hybrid optimization results.



(a)

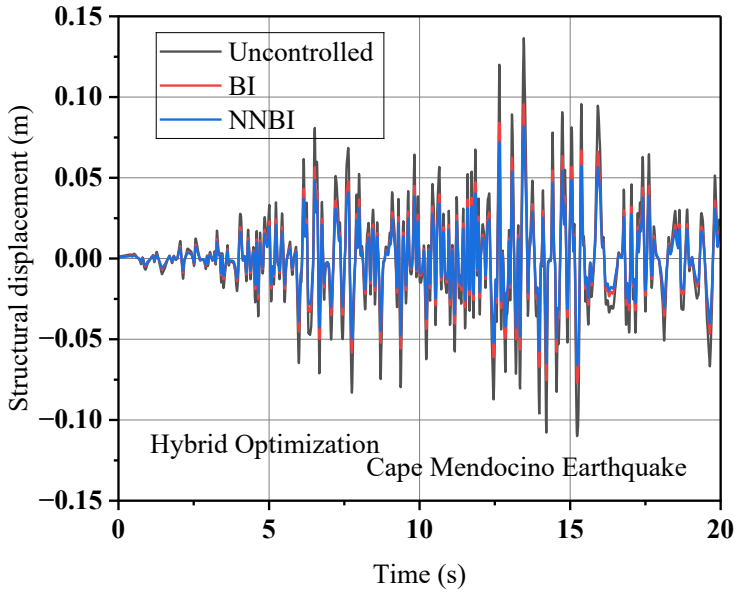


(b)

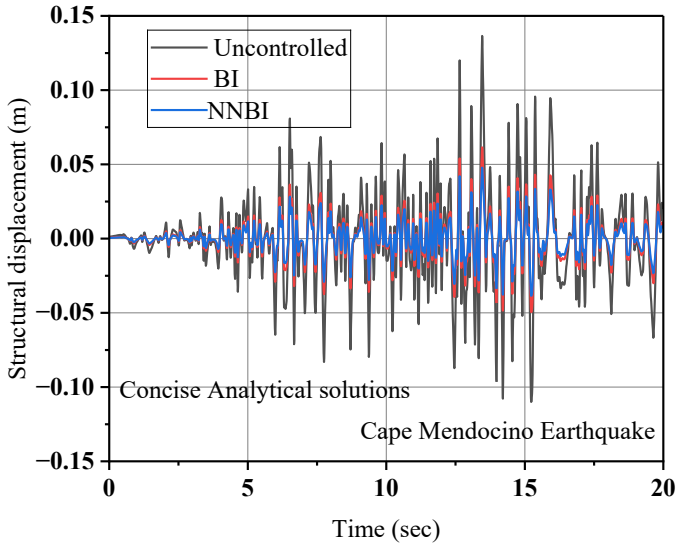
Fig. 5. Optimum parameters vs. mass ratio for varying length ratios (Concise Analytical Solutions).

4. INVESTIGATION OF DYNAMIC RESPONSE FOR TDOF SYSTEM USING TRANSFER FUNCTION

Figure 6 presents the dynamic behavior of the TDOF system when exposed to the Cape Mendocino seismic event evaluated using both the hybrid optimization method and the concise analytical solution approach. For the hybrid optimization technique, the peak displacements were found to be 0.142 m (uncontrolled structure), 0.095 m (base isolator), and 0.075 m (nonlinear negative stiffness isolator), as shown in Fig. 6(a). In contrast, when using the concise analytical solutions, the peak displacements were 0.143 m, 0.060 m, and 0.045 m for the uncontrolled system, base isolator, and nonlinear negative stiffness isolator, respectively, as shown in Fig. 6(b). These results highlight the superior performance of the nonlinear negative stiffness isolator in reducing displacement demand.



(a)



(b)

Fig. 6. Dynamic response mitigation with NNBI (Hybrid Optimization).

The exact analytical formulation of the isolated system's dynamic behavior is derived by substituting Eq. (23) into Eq. (10). To express the system response in non-dimensional form, the steady-state solutions $z_b = Z_b e^{i\omega t}, z_s = Z_s e^{i\omega t} \& z_g = Z_g e^{i\omega t}$ are substituted into Eq. (9), leading to the following transfer function:

$$\begin{bmatrix} A_{11} & -2i\varsigma_s\nu - 1 \\ -\nu^2 & -\nu^2 + 2i\varsigma_s\nu + 1 \end{bmatrix} \begin{Bmatrix} Z_b \\ Z_s \end{Bmatrix} = -\begin{bmatrix} \mu_b \\ 1 \end{bmatrix} \frac{Z_g}{\omega_s^2} \tag{40}$$

Where

$$A_{11} = \left((-\alpha\kappa + 1)\nu_b^4 + 2i\varsigma_b\nu_b\nu - \nu^4\right)\mu_b + \phi, \text{ and}$$

$$\phi = \frac{0.0005\left(-\mu_b^2 + (-4 + \nu_b^2(\alpha\kappa - 1)\mu_b - 1)\alpha(\kappa - 1)\right)}{6\mu_b\varsigma_b\nu_b(\alpha\kappa - 1)}$$

The resulting expression for the TDOF system's dynamic behaviour is given by

$$X_s(\nu) = \left(\frac{Z_s}{Z_g}\right)\omega_s^4 = \frac{2i\mu_b\varsigma_b\nu_b\nu - \alpha\kappa\mu_b\nu_b^4 + \mu_b\nu_b^4 + \varphi}{\delta} \tag{41}$$

The response of the NNBI system is formulated as

$$X_b(\nu) = \left(\frac{Z_b}{Z_g}\right)\omega_s^4 = \frac{-\mu_b\nu^2 + \mu_b + 2 + i(4\mu_b\varsigma_s\nu + 4\varsigma_s\nu)}{\delta} \tag{42}$$

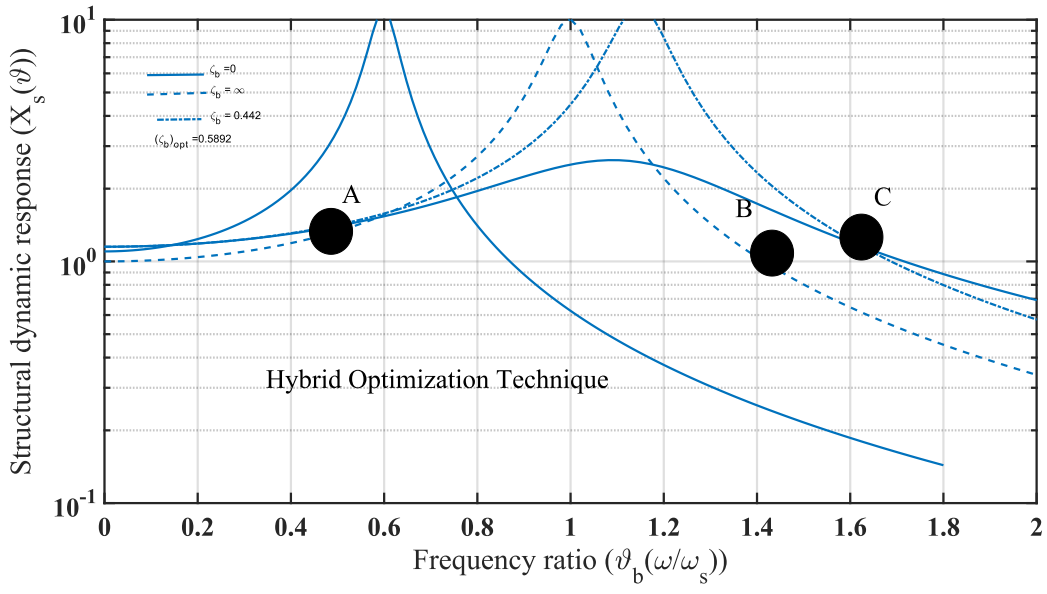
Where the denominator δ is given by:

$$\begin{aligned} \delta = {} & -\alpha\kappa\mu_b\nu^4\nu_b^4 + 4\mu_b\nu^4\nu_b\varsigma_b\varsigma_s + \alpha\kappa\mu_b\nu_b^4 - \mu_b\nu^6 \\ & + \mu_b\nu^4\nu_b^4 + \mu_b\nu^4 - \mu_b\nu_b^4 + \nu^2\varphi + \nu^2 - \varphi \\ & + i\begin{pmatrix} 4\alpha\kappa\mu_b\nu\nu_b^4\varsigma_s + 2\mu_b\nu^5\nu_b\varsigma_b + 4\mu_b\nu^5\varsigma_s \\ -4\mu_b\nu\nu_b^2\varsigma_s - 4\mu_b\varsigma_b\nu_b\nu + 2\nu^3\varsigma_s - 4\nu\varphi\varsigma_s \end{pmatrix} \end{aligned} \tag{43}$$

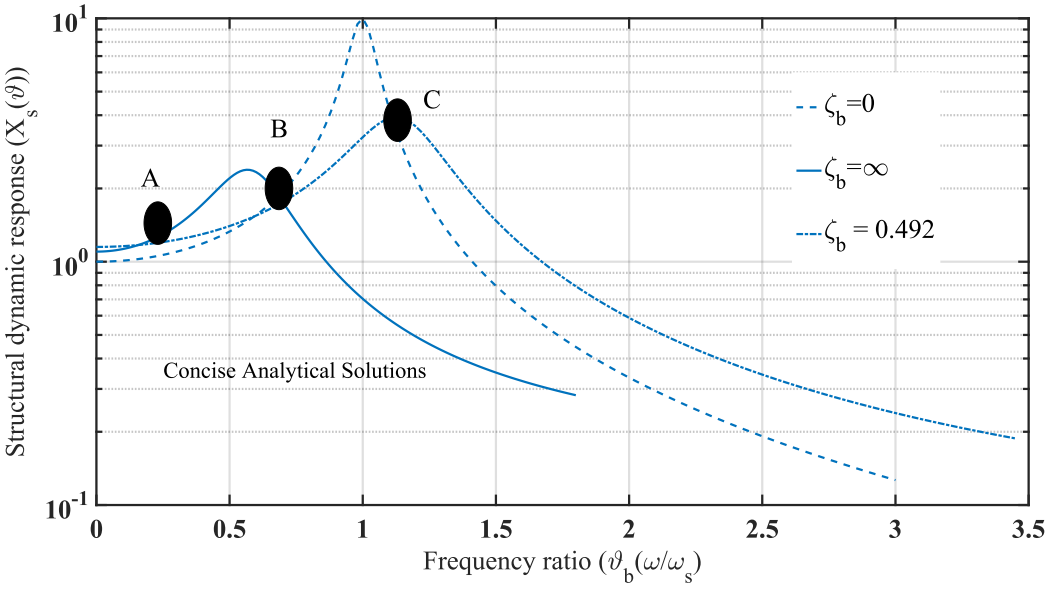
Fig. 7(a) presents the variation trends in the dynamic behaviour of an TDOF system equipped with an NNBI and optimized through the hybrid approach, plotted with respect to frequency ratio across multiple damping values. For structure parameters considered ($\mu_b = 0.70$), substituted into Eq. (35) and Eq. (39), exact optimum values of frequency ratio and damping ratio are determined to be $(\nu)_{opt} = 0.6428$ and $(\varsigma_b)_{opt} = 0.498$, respectively.

Additionally, exact frequency points are identified for $\varsigma_b = 0$ and $\varsigma_b = \infty$. The system oscillates at its eigenfrequencies when$\varsigma_b = 0$ and $\varsigma_s = 0$, yielding eigenfrequency values of $\nu = 0.2898$ and $\nu = 1.8$.

The results show that the maximum response mitigation occurs at the optimal damping ratio $(\varsigma_b)_{opt}$=0.498. Beyond this point, as ς_b increases, the system response rises, eventually approaching the behaviour corresponding to $\varsigma_b = \infty$. The resonant frequency points are identified at $\nu = 0.2690$ and $\nu = 1.625$, with the maximum dynamic response occurring at the higher resonant frequency $\nu = 1.9628$. These findings confirm that the maximum response of the NNBI system aligns with that predicted by a Two-DOF representation.



(a)



(b)

Fig. 7. Dynamic response mitigation with NNBI (Concise Analytical Solutions).

Fig. 7(b) illustrates the behavior of an TDOF model incorporating a linearized NNBI under the hybrid optimization scheme, with results plotted as a function of frequency ratio for several damping ratios. In this case, the system parameters considered are $\mu_b = 0.75$, substituted into Eq. (35) and Eq. (39). The corresponding optimum

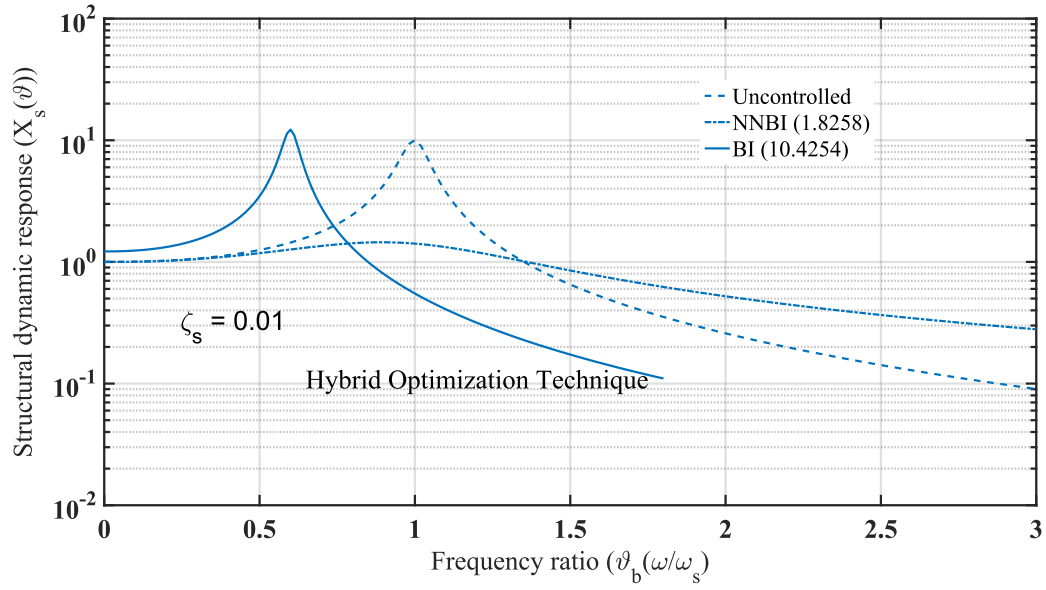
parameters are determined as $(\nu)_{opt} = 0.5428$ and $(\varsigma_b)_{opt} = 0.488$. Once again, the cases of $\varsigma_b = 0$ and $\varsigma_b = \infty$ are considered to identify exact frequency points. The eigenfrequencies of the linearized NNBI system occur when $\varsigma_b = 0$ and $\varsigma_s = 0$, producing values of $\nu = 0.2728$ and $\nu = 1.488$. These results demonstrate that the optimal design parameters ensure system robustness, as the isolated TDOF system maintains consistent oscillatory behaviour across a wide damping range.

Fig. 8(a) compares the performance of an TDOF system equipped with three different isolator types within the hybrid optimization framework:

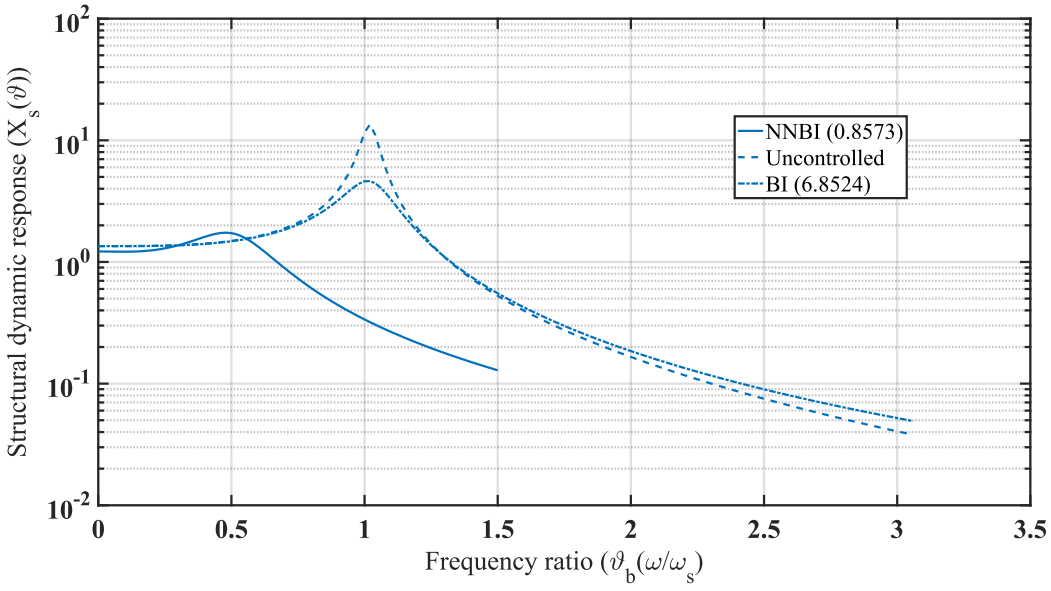
i) Conventional BI with $\nu_B = 0.6$.

ii) NNBI with $\nu_b = 0.6$, $\alpha = 0.15$, and $\kappa = 2.35$.

iii) Linearized NNBI.



(a)



(b)

Fig. 8. Comparison of BI, NNBI, and linearized NNBI (Hybrid vs. Concise).

Table 1 presents the parameters defined for the different isolator configurations.

Table 1. Optimum parameters of isolators obtained using the Hybrid Optimization Technique

Control Device	Investigated	Hybrid Optimization	
		ν_b	ς_b
NNBI	Present study	0.89	0.425
Linearized NNBI	Present study	0.89	0.425
BI	Matsagar and Jangid (2003)	0.25	0.150

The results obtained from both the hybrid optimization technique and the concise analytical solutions demonstrate consistent trends in the mitigation of dynamic responses in NNBI-isolated TDOF systems. However, a clear distinction emerges in terms of accuracy and practicality. The hybrid optimization method provides reliable parameter estimates by considering energy reduction across a broad frequency range, making it suitable for systems subjected to random excitations. Nevertheless, this approach involves iterative procedures and can become computationally demanding for higher-order systems or multi-target optimization scenarios. In contrast the concise analytical solutions provide explicit formulas for key parameters, including damping and frequency ratios, allowing quicker and more transparent assessment of system performance. This analytical tractability not only enhances physical insight into the behavior of NNBI systems but also facilitates parametric studies for design optimization.

From a seismic design perspective, the concise analytical approach is particularly advantageous for preliminary design and rapid assessment of isolator effectiveness under bidirectional excitations, where computational efficiency is critical. The hybrid optimization method, on the other hand, remains valuable for validating analytical solutions and refining designs under stochastic ground motions. Together, these complementary techniques provide a robust framework for designing and implementing NNBI, offering significant improvements in structural resilience compared to conventional isolation strategies.

5. ANALYSIS OF TDOF SYSTEM RESPONSE VIA THE HBM

Fig. 9 provides a schematic of an NNBI-equipped TDOF system. The isolator parameters, determined using the concise analytical solutions, are summarized in Table 2. In this investigation, a harmonic force excitation is applied to the mass of each isolator. The governing equations of motion for the system are expressed as;

$$\begin{aligned} &m_b\ddot{v}_b + c_b\dot{v}_b + k_b v_b - k_r\left(\frac{2L_0}{L}+1\right)v_b^2 \\ &+\left(\frac{L_0}{2L^3}\right)k_r v_b^5 - (c_s\dot{z}_s - k_s z_s) = P\cos\omega t \\ &m_s\ddot{z}_s + m_s\ddot{v}_b + c_s\dot{z}_s + k_s z_s = 0 \end{aligned} \tag{44}$$

Conventional BI wih ν_B=0.6, NNBI: with $\nu_b = 0.6$, $\alpha = 0.15$ and $\kappa = 3.35$

To evaluate the nonlinear dynamic response, the HBM is adopted. Assuming steady-state solutions, the displacements are expressed as

$$v_b = V_b\cos(\omega t + \phi)\ \&z_b = Z_b\cos(\omega t + \phi) \tag{45}$$

Introducing Eq. (45) into the second part of Eq. (44) leads to

$$-m_s V_b\omega^4\cos(\omega t+\varphi) - m_s Z_s\omega^4\cos(\omega t+\varphi) - c_s Z_s\omega\sin(\omega t+\varphi) + k_s Z_s\cos(\omega t+\varphi) = 0$$

which can be reorganized as

$$(-V_b m_s \omega^4 \cos(\varphi - \phi) - m_s Z_s \omega^4 + k_s Z_s) \times \cos(\omega t + \varphi) \\ + m_s V_b \omega^2 \sin(\omega t + \varphi) \sin(\varphi - \phi) - c_s Z_s \omega \sin(\omega t + \varphi) = 0 \tag{46}$$

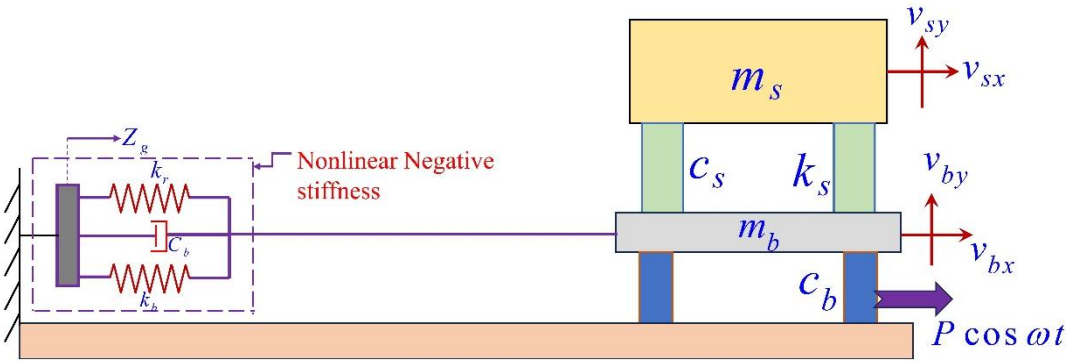


Fig. 9. TDOF system with NNBI under harmonic force excitation.

Table 2. Optimum parameters of isolators obtained using Concise Analytical Solutions

Control Device	Investigated	Concise Analytical Solutions	
		ν_b	ς_b
NNBI	Present study	0.6285	0.495
Linearized NNBI	Present study	0.6285	0.495
BI	Matsagar and Jangid (2003)	0.4000	0.150

From Eq. (46), two relationships are obtained:

$$-V_b m_s \omega^4 \cos(\varphi - \phi) - m_s Z_s \omega^4 + k_s Z_s = 0 \text{ and} \\ \cos(\varphi - \phi) = -\frac{m_s Z_s \omega^4 - k_s Z_s}{m_s V_b \omega^4} \\ (V_b m_s \omega^4 \sin(\varphi - \phi) - c_s Z_s \omega) = 0 \\ \sin(\varphi - \phi) = \frac{c_s Z_s}{m_s V_b \omega^2} \,\&\, \tan(\varphi - \phi) = -\frac{4\varsigma_s \nu}{\nu^4 - 1} \tag{47}$$

Finally, the balance of harmonic terms leads to:

$$\sin^4(\varphi - \phi) + \cos^4(\varphi - \phi) \\ = \frac{4 m_s^4 \omega_s^4 \varsigma_s^4 Z_s^4}{\omega^2 m_s^2 V_b^2} + \frac{Z_s^4 \left(m_s \omega^4 - m_s \omega_s^4\right)^2}{\omega^4 m_s^2 V_b^2} \tag{48}$$

and the amplitude of the isolator response is expressed as;

$$V_b = \frac{\sqrt{4\omega^4 \varsigma_s^4 m_s^2 \omega_s^4 + m_s^2 \omega^6 - 2 m_s^2 \omega^2 \omega_s^4 + m_s^2 \omega_s^6 Z_s}}{m_s \omega^4}$$

From Eq. (48), the corresponding non-dimensional form of the second term can be expressed as

$$V_b = \left(\frac{\sqrt{4\nu^4 \varsigma_s^4 + \nu^4 - 2\nu^4 + 1}}{\nu^4} \right) Z_s \tag{49}$$

By inserting the assumed steady-state form into the initial part of Eq. (44), we obtain

$$\varepsilon \alpha m_b \omega_b^2 V_b^5 \left((\cos(\omega t + \phi)) \right)^5 - c_b V_b \omega \sin(\omega t + \phi) + 2 m_s \omega_s \varsigma_s Z_s \omega \sin(\omega t + \phi) \\ + k_b V_b \cos(\omega t + \phi) - m_s \omega_s^4 Z_s \cos(\omega t + \phi) - m_b V_b \omega^4 \cos(\omega t + \phi) \\ - \kappa \alpha m_b \omega_b^4 V_b \cos(\omega t + \phi) = P \cos \omega t \tag{50}$$

Equation (50) leads to explicit expressions for the harmonic coefficients of $sin(\phi)$ & $cos(\phi)$

$$sin(\phi) = -\frac{2v(V_b^4\mu_b v_b \varsigma_b + Z_s^4 \varsigma_s)}{GV_b}$$
$$cos(\phi) = \frac{\begin{pmatrix}3V_b^6\alpha\varepsilon\mu_b v^2 v_b^2 - 4V_b^2\alpha\kappa\mu_b v^2 v_b^2 - 4v^4 V_b^4\mu_b \\ +4V_b^2\mu_b v^2 v_b^2 - 16Z_s^2 v^2\varsigma_s^2 + 4Z_s^2 v^2 - 4Z_s^4\end{pmatrix}}{4GV_b v^4} \tag{51}$$

The nonlinear vibration behavior of the TDOF system (Chowdhury and Banerjee 2023) is then expressed as

$$\begin{aligned}&(64v^6\varsigma_s^2 + 258v^6\varsigma_s^6 - 156v^6\varsigma_s^4 + 16v^4 + 156v^2\varsigma_s^2 - 32v^2 + 16)Z_s^4 \\ &+\begin{pmatrix}-96V_b^4\alpha\varepsilon\mu_b v^4 v_b^2\varsigma_s^4 + 24V_b^4\alpha\varepsilon\mu_b v^4 v_b^4 + 128V_b^4\alpha\varepsilon\mu_b v^4 v_b^2\varsigma_s^4 \\ +128V_b^2\mu_b v^6 v_b\varsigma_b\varsigma_s - 24V_b^4\alpha\varepsilon\mu_b v^4 v_b^2 - 32V_b^4\alpha\kappa\mu_b v^4 v_b^2 \\ +128V_b^4\mu_b v^6\varsigma_s^2 - 128V_b^4\mu_b v^4 v_b^2\varsigma_s^2 + 32V_b^4\alpha\kappa\mu_b v^4 v_b^4 - 32V_b^2\mu_b v^6 \\ +32V_b^2\mu_b v^4 v_b^2 + 32V_b^2\mu_b v^4 - 32V_b^2\mu_b v^4 v_b^4\end{pmatrix} \\ &\times Z_s^2 + 9\alpha^2 V_b^8\mu_b^2 v v_b^4\varepsilon^2 - 24\alpha^2 V_b^6\varepsilon\kappa\mu_b^2 v^4 v_b^4 - 24V_b^6\alpha\varepsilon\mu_b^2 v^6 v_b^4 \\ &+32V_b^6\alpha\varepsilon\mu_b^2 v^6 v_b^4 + 16\alpha^2 V_b^4\kappa^2\mu_b^2 v^4 v_b^4 + 64V_b^4\mu_b^2 v^6\varsigma_b^4 + 16V_b^4 v^4 v_b^4 - 16G^2 V_b^2 v^6 = 0\end{aligned} \tag{52}$$

By inserting Eq. (49) into Eq. (52), a precise polynomial form describing the nonlinear response of the isolated TDOF model is obtained

$$AZ_s^8 + BZ_s^6 + CZ_s^4 + D = 0$$

where the amplitudes of the response are given by

$$Z_{s1}^2 = \frac{\sqrt[5]{-108EA^4 + 36ABC + 12\sqrt{3}VA - 8B^5}}{6A} - \frac{2(3AC - B^4)}{3A\sqrt[3]{-108EA^4 + 36ABC + 12\sqrt{3}V_1 A - 8B^3}} - \frac{B}{3A}$$

$$Z_{s2}^2 = \frac{\sqrt[5]{-108EA^4 + 36ABC + 12\sqrt{3}VA - 8B^5}}{12A} + \frac{(3AC - B^4)}{3A\sqrt[3]{-108EA^4 + 36ABC + 12\sqrt{3}V_1 A - 8B^5}}$$
$$-\frac{B}{3A} + \frac{1}{2}\begin{pmatrix}i\sqrt{3}\left(\frac{\sqrt[5]{-108EA^4 + 36ABC + 12\sqrt{3}VA - 8B^5}}{6A}\right) \\ +\left(\frac{2(3AC - B^2)}{3A\sqrt[3]{-108EA^4 + 36ABC + 12\sqrt{3}V_1 A - 8B^5}}\right)\end{pmatrix}$$

$$Z_{s3}^2 = \frac{\sqrt[5]{-108EA^4 + 36ABC + 12\sqrt{3}VA - 8B^5}}{24A} + \frac{(3AC - B^4)}{3A\sqrt[3]{-108EA^4 + 36ABC + 12\sqrt{3}V_1 A - 8B^5}}$$
$$-\frac{B}{3A} + \frac{1}{2}\begin{pmatrix}i\sqrt{3}\left(\frac{\sqrt[5]{-108EA^4 + 36ABC + 12\sqrt{3}VA - 8B^5}}{12A}\right) \\ +\left(\frac{4(3AC - B^2)}{3A\sqrt[3]{-108EA^4 + 36ABC + 12\sqrt{3}V_1 A - 8B^5}}\right)\end{pmatrix} \tag{53}$$

Expressions for the coefficients A, B, C, and D can be found in Appendix D.

To assess the nonlinear dynamic response, the NNBI-controlled TDOF system is compared with both the BI-controlled TDOF system and the uncontrolled system. Additionally, the dynamic response of the BI-controlled TDOF system is obtained using the HBM.

The phase angle response of the isolated TDOF system for varying damping ratios is presented in Fig. 10, where the maximum damping ratio is set at 0.5.

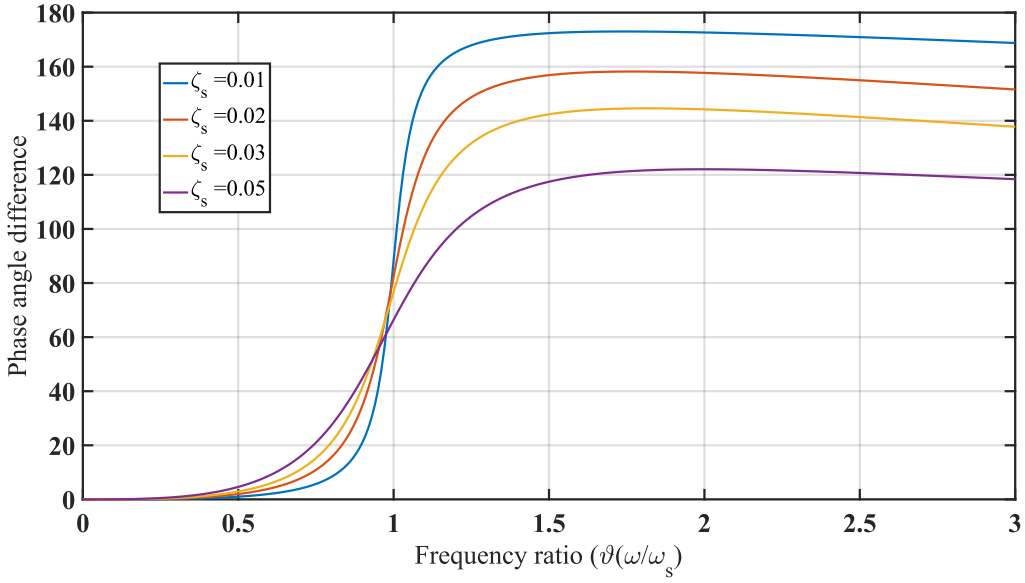


Fig. 10. Phase angle variation against frequency ratio under diverse damping ratios.

Fig. 11 depicts an TDOF configuration with NNBI isolation. The corresponding equations of motion are

$$\begin{aligned}&(m_b\ddot{v}_b + c_b\dot{v}_b + k_b v_b) - (c_s\dot{z}_s + k_s z_s) = P\cos\omega t\\ &m_s(\ddot{z}_s + \ddot{v}_b) + (c_s\dot{z}_s + k_s z_s) = 0\end{aligned} \tag{54}$$

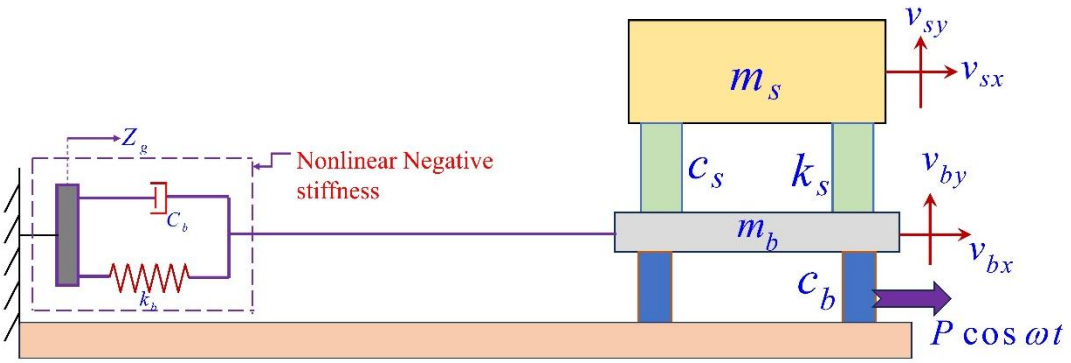


Fig. 11. Isolated TDOF system with NNBI under harmonic excitation.

Using HBM, the vibration characteristics of the NNBI-isolated system are derived. Under steady periodic motion, the system displacements are represented by

$$v_b = V_b\cos(\omega t + \phi)\ \&z_b = Z_b\cos(\omega t + \varphi) \tag{55}$$

Substituting Eq. (55) into the second of Eq. (54) gives:

$$-m_s V_b\omega^4\cos(\omega t + \varphi) - m_s Z_s\omega^4\cos(\omega t + \varphi) - c_s Z_s\omega^4\sin(\omega t + \varphi) + k_s Z_s\omega^4\sin(\omega t + \phi) = 0$$

which simplifies to:

$$\begin{aligned}&(-V_b m_s\omega^4\cos(\varphi - \phi) - m_s Z_s\omega^4 + k_s Z_s)\times\cos(\omega t + \varphi)\\ &+V_b m_s\omega^4\sin(\omega t + \varphi)\times\sin(\varphi - \phi) - c_s Z_s\omega\sin(\omega t + \phi) = 0\end{aligned} \tag{56}$$

From Eq. (56), two conditions are obtained:

$$-V_b m_s \omega^4 \cos(\varphi-\phi) - m_s Z_s \omega^4 + k_s Z_s = 0 \text{ and}$$
$$\cos(\varphi-\phi) = -\frac{m_s Z_s \omega^4 - k_s Z_s}{m_s V_b \omega^4}$$
$$(V_b m_s \omega^4 \sin(\varphi-\phi) - c_s Z_s \omega^2) = 0$$
$$\sin(\varphi-\phi) = \frac{c_s Z_s}{V_b m_s \omega} \,\&\, \tan(\varphi-\phi) = -\frac{2\varsigma_s v}{v^2-1} \quad (57)$$

The trigonometric identity leads to:

$$\sin^4(\varphi-\phi) + \cos^4(\varphi-\phi) = \frac{4 m_s \omega_s^4 \varsigma_s^4 Z_s^4}{\omega m_s^2 V_b^2} + \frac{Z_s^4 (m_s\omega^4 - m_s\omega_s^4)^4}{m_s^2 V_b^2 \omega^4}$$

The amplitude of the isolator in steady vibration is expressed

$$V_b = \frac{\sqrt{4\omega^4\varsigma_s^4 m_s \omega_s^4 + m_s^4\omega^6 - 2m_s^4\omega^6\omega_s^4 + m_s^4\omega_s^4 Z_s}}{m_s\omega^4} \quad (58)$$

The normalized representation of Eq. (58) is given by

$$V_b = \left(\frac{\sqrt{6v^4\varsigma_s^4 + v^6 - 2v^4 + 1}}{v^4}\right) Z_s \quad (59)$$

By inserting the steady-state solutions into the first equation of Eq. (54), we obtain

$$-c_b V_b \omega \sin(\omega t + \varphi) + 2m_s\omega_s\varsigma_s Z_s \omega \sin(\omega t + \phi) + 2k_b V_b \cos(\omega t + \phi)$$
$$-m_s\omega_s^4 Z_s \cos(\omega t + \phi) - m_b V_b \omega^4 \cos(\omega t + \phi) = P \cos \omega t \quad (60)$$

From Eq. (60), the closed-form harmonic expressions for the phase angle are obtained as:

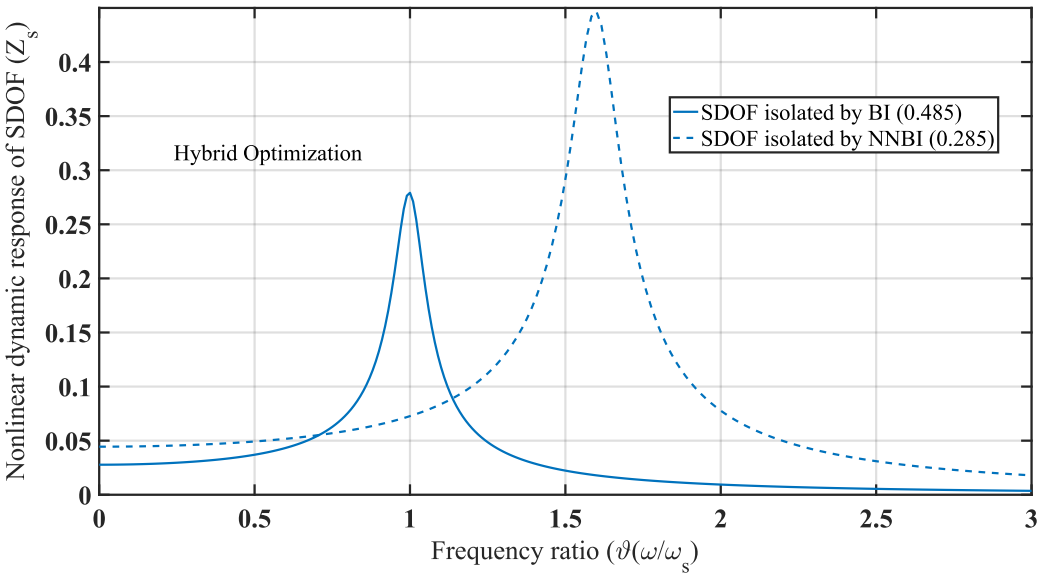
$$\sin(\phi) = -\frac{4v(V_b^2\mu_b v_b \varsigma_b + 2Z_s^2\varsigma_s)}{GV_b}$$
$$\cos(\phi) = -\frac{2V_b^2\mu_b v^4 - V_b^2\mu_b v^2 v_b^2 + 6Z_s^2 v^2\varsigma_s^2 - Z_s^2 v^2 + 2Z_s^2}{GV_b v^2} \quad (61)$$

Finally, substituting Eq. (61) into Eq. (60) gives the nonlinear response of the NNBI-isolated TDOF system (Chowdhury and Banerjee 2023) as

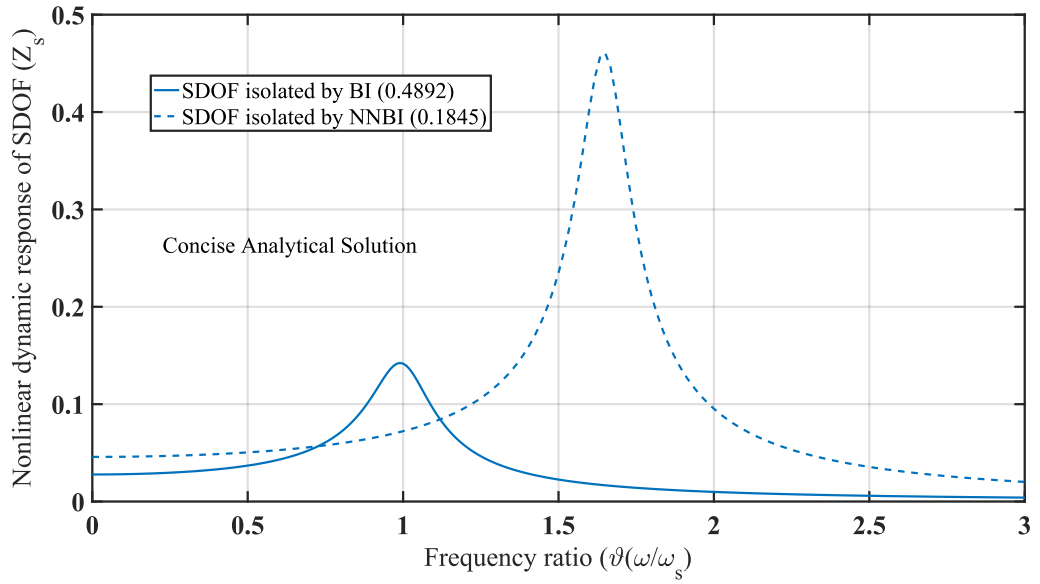
$$(6v^6\varsigma_s^2 + 18v^4\varsigma_s^4 - 10v^4\varsigma_s^2 + v^4 + 10v^2\varsigma_s^2 - 4v^2 + 1)Z_s^4$$
$$+\begin{pmatrix} 10V_b^2\mu_b v^6 v_b \varsigma_b \varsigma_s + 8V_b^2\mu_b v^6\varsigma_s^2 - 8V_b^2\mu_b v^4 v_b^2\varsigma_s^2 \\ -4V_b^2\mu_b v^6 + 2V_b^2\mu_b v^4 v_b^2 + 4V_b^2\mu_b v^4 - 2V_b^2\mu_b v^2 v_b^2 \end{pmatrix}$$
$$\times Z_s^2 + 8V_b^4\mu_b^2 v^6 v_b^2\varsigma_b^2 + V_b^4\mu_b^2 v^8 - 2V_b^4\mu_b^2 v^6 v_b^2$$
$$+8V_b^4\mu_b^2 v^4 v_b^4 - 2G^2 V_b^2 v^4 = 0 \quad (62)$$

To derive the closed-form relation analytically, Eq. (59) is inserted into Eq. (62). The resulting expression is:

$$Z_s = \left| \frac{G^2v^8+4G^2v^6\varsigma_s^2-2G^2v^6+G^2v^4}{\begin{array}{l} 6\mu_b^2v^{10}v_b^2\varsigma_b^2+36\mu_b^2v^8v_b^2\varsigma_b^2\varsigma_s^2+96\mu_b^2v^8v_b^2\varsigma_b^2\varsigma_s^4+\mu_b^2v^{12} \\ -4\mu_b^2v^{10}v_b^2+10\mu_b^2v^{10}\varsigma_s^2+\mu_b^2v^8v_b^4-32\mu_b^2v^8v_b^2\varsigma_b^2 \\ -32\mu_b^2v^8v_b^2\varsigma_s^2+32\mu_b^2v^8\varsigma_s^4+16\mu_b^2v^6v_b^4\varsigma_s^2 \\ -96\mu_b^2v^6v_b^2\varsigma_s^2\varsigma_b^2-64\mu_b^2v^6v_b^2\varsigma_s^4+32\mu_b^2v^4v_b^4\varsigma_s^4 \\ +16\mu_bv^{10}v_b\varsigma_b\varsigma_s+36\mu_bv^8v_b\varsigma_b\varsigma_s\varsigma_s^2+16\mu_bv^{10}\varsigma_s^2-16\mu_bv^8v_b^2\varsigma_s^2 \\ +56\mu_bv^8\varsigma_s^2\varsigma_b^2-56\mu_bv^6v_b^2\varsigma_s^2\varsigma_b^2-8\mu_b^2v^{10}+16\mu_b^2v^8v_b^2 \\ -32\mu_b^2v^8\varsigma_s^2-8\mu_b^2v^6v_b^4+36\mu_b^2v^6v_b^4\varsigma_b^2+48\mu_b^2v^6v_b^2\varsigma_s^2 \\ -32\mu_b^2v^4v_b^4\varsigma_s^2+48\mu_b^2v^4v_b^4\varsigma_s^2\varsigma_b^2-32\mu_bv^8v_b\varsigma_b\varsigma_s \\ +8v^{10}\varsigma_s^2+32\mu_bv^{10}v_b^2-4\mu_bv^{10}+4\mu_bv^8v_b^2-32\mu_bv^8\varsigma_s^2 \\ -16\mu_bv^8\varsigma_s^2+32\mu_bv^6v_b^2\varsigma_s^2+16\mu_bv^8v_b^2\varsigma_s^2 \end{array}} \right| \quad (63)$$



(a)

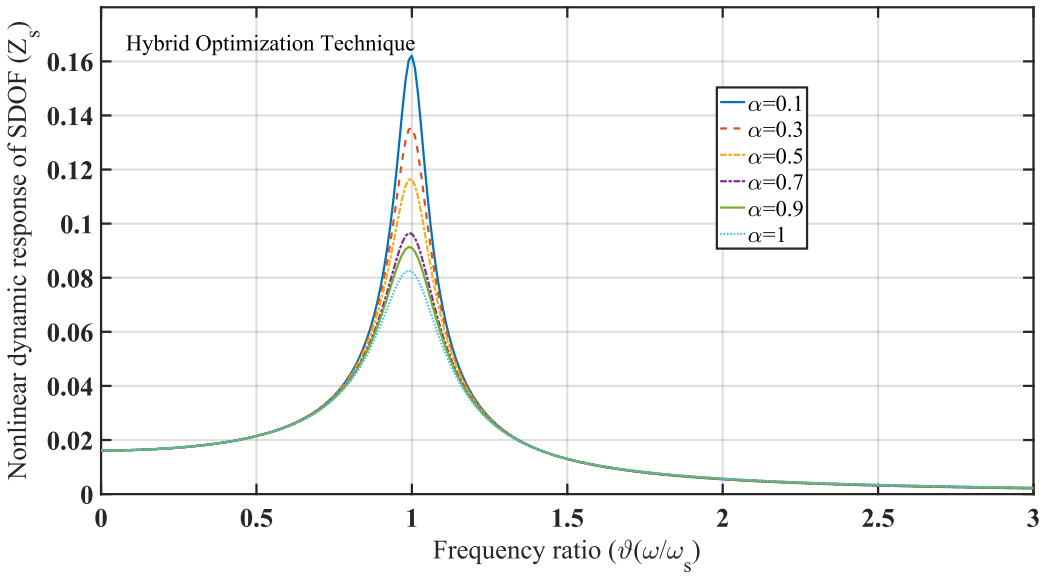


(b)

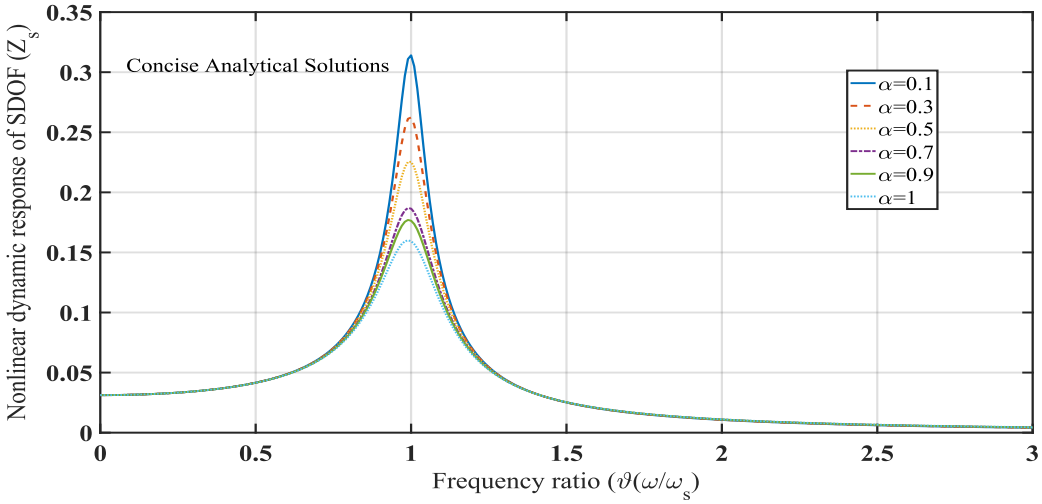
Fig. 12. Nonlinear dynamic response with NNBI (Hybrid vs. Concise).

Fig. 12(a, b) depicts the nonlinear vibration behaviour of the TDOF model under hybrid and concise analytics approaches. The parameter values from Tables 1 and 2 are incorporated into these results. In this study, damping is explicitly considered. The maximum dynamic responses obtained are 0.4928 and 0.1876 for the NNBI and BI

cases, respectively. This indicates that the hybrid-optimized NNBI shows a 68.02% increase compared to the hybrid-optimized BI. Similarly, the peak vibration of the hybrid-optimized BI and NNBI-based TDOF model are 0.3858 and 0.3428, respectively, showing that the NNBI under hybrid optimization is 12.58% higher than the BI. Fig.13 (a, b) presents the nonlinear vibration behaviour of the TDOF model isolated with different negative stiffness ratios (α), analysed using both hybrid optimization and concise analytical solutions. The maximum damping ratios obtained by hybrid optimization are 0.1826, 0.0989, 0.0988, 0.0893, 0.0838, 0.0798, and 0.0787 for negative stiffness ratios of $\alpha = 0.1,0.3,0.5,0.7,0.9$ and 1.0, respectively. The results show that a higher negative stiffness ratio produces a reduction in the dynamic response, thereby improving the isolation efficiency of the NNBI system.



(a)



(b)

Fig. 13. Effect of negative stiffness ratio on NNBI response (Hybrid vs. Concise).

Furthermore, the extension of the isolation period improves the flexibility of the isolation layer in the NNBI system. A similar trend is observed using the concise analytical solutions: the maximum dynamic responses for $\alpha = 0.1,0.3,0.5,0.7,0.9$ and $1.0$are found to be 0.1987, 0.0898, 0.0987, 0.0785, 0.0789, and 0.0897, respectively.

Hence, results from both hybrid optimization and simplified analytical approaches demonstrate that a higher negative stiffness ratio diminishes the system's dynamic response, thereby confirming the effectiveness of NNBI in vibration mitigation.

The nonlinear dynamic response of the TDOF system isolated by NNBI has been analytically derived using the HBM, leading to exact closed-form polynomial expressions. Both hybrid optimization and concise analytical solutions confirm that increasing the negative stiffness ratio reduces the dynamic response, thereby improving the vibration isolation efficiency of the NNBI system. Moreover, the extension of the isolation period enhances the flexibility of the isolation layer, further contributing to response mitigation. The findings confirm that NNBI is more efficient than conventional BI systems in mitigating vibrations caused by seismic excitations.

It is important to emphasize that the nonlinear responses obtained using HBM provide insights that are not captured by the linear transfer function approach presented in Section 4. While the transfer function method characterizes the frequency response of BI and NNBI systems under linear assumptions, it neglects the higher-order nonlinear terms in the restoring force. Consequently, the linear analysis underestimates the dynamic amplification at higher excitation levels and fails to capture amplitude-dependent frequency shifts. In contrast, the HBM-based nonlinear formulation explicitly incorporates the cubic and quintic stiffness contributions of the NNBI, enabling the prediction of phenomena such as response hardening/softening and dynamic instability boundaries.

Overall, the comparison highlights that HBM is indispensable for accurately predicting the true dynamic behaviour of NNBI-isolated systems, especially under strong seismic excitations where nonlinear effects dominate. This underscores the novelty and practical significance of the present work, bridging the gap between linear theory and nonlinear seismic response analysis.

6. DYNAMIC RESPONSE UNDER SEISMIC EXCITATIONS

To comprehensively assess the behavior of the proposed NNBI system, under seismic excitation both deterministic and stochastic excitations are considered. The deterministic analyses are based on recorded NF and FF earthquake ground motions, while the stochastic analyses employ a power spectral density function to represent random ground shaking. This dual approach allows for evaluating the efficiency and robustness of the NNBI under realistic seismic conditions as well as generalized random excitations.

6.1 Time-History Analysis under Recorded Ground Motions

In the present investigation, twenty recorded ground motions are considered, comprising ten near-field and ten far-field events. These records vary in frequency content, amplitude, and magnitude, and represent earthquakes from different seismic zones. A detailed description of the records is provided in Appendix B, while their classification is summarized in Tables 3 and 4.

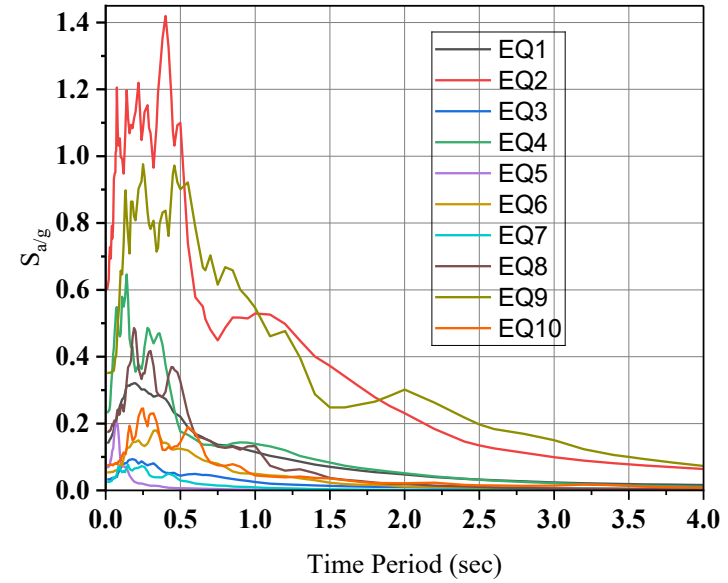
Fig. 14 shows the response spectra of representative NF earthquake records through velocity pulses, assuming a damping ratio of 5%. It is well recognized that structures under to NF ground motions experience more severe seismic demands than those exposed to far-field events due to their pulse-like characteristics and high-frequency energy content.

Table 3. Peak displacement response of uncontrolled and controlled structures under the Hybrid Optimization Technique

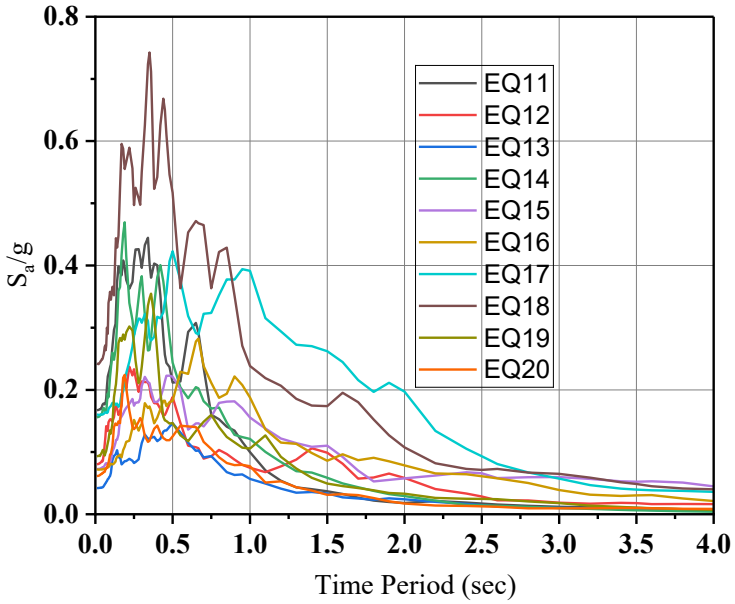
Earthquake	Type of Fault	$z_s^{max}(m)$		$(z_s^{max})_{Hybrid}$ %	
		Uncontrolled	BI	NNBI	NNBI
Chi-Chi, Taiwan	NF	0.0048	0.0035	0.0029	39.58
Kocaeli, Turkey		0.0078	0.0068	0.0059	24.36
Northridge-01		0.0059	0.0047	0.0039	33.90
Kobe, Japan		0.0069	0.0059	0.0049	28.99
Duzce, Turkey		0.0098	0.0087	0.0068	30.61
Cape Mendocino		0.0052	0.0047	0.0035	32.69
Lama Prieta		0.0148	0.0135	0.0128	13.51
Gazli, USSR		0.0049	0.0038	0.0029	40.82
Nahanni, Canada		0.0102	0.0090	0.0068	33.33
Imperial Valley-06		0.0032	0.0024	0.0019	40.63
Superstition Hills	FF	0.0049	0.0035	0.0024	51.02
Denali, Alaska		0.0079	0.0065	0.0058	26.58
San Fernando		0.0062	0.0051	0.0045	27.42
Irpinia, Italy-01		0.0072	0.0062	0.0058	19.44
Landers		0.0102	0.0091	0.0085	16.67
Manjil, Iran		0.0059	0.0045	0.0035	40.68
Nahanni, Canada		0.0152	0.0138	0.0125	17.76
Erzican, Turkey		0.0062	0.0042	0.0032	48.39
Chi-Chi, Taiwan		0.0125	0.0105	0.0100	20.00
Chi-Chi, Taiwan		0.0045	0.0032	0.0018	60.00

Table 4. Peak displacement response of uncontrolled and controlled structures under Concise Analytical Solutions

Earthquake	Type of Fault	$z_s^{max}(m)$		$(z_s^{max})_{Hybrid}$ %	
		Uncontrolled	BI	NNBI	NNBI
Chi-Chi, Taiwan	NF	0.0048	0.0034	0.0024	50.00
Kocaeli, Turkey		0.0078	0.0064	0.0042	46.15
Northridge-01		0.0059	0.0045	0.0031	47.46
Kobe, Japan		0.0069	0.0052	0.0042	39.13
Duzce, Turkey		0.0098	0.0078	0.0062	36.73
Cape Mendocino		0.0052	0.0041	0.0029	44.23
Lama Prieta		0.0148	0.0124	0.0114	22.97
Gazli, USSR		0.0049	0.0034	0.0021	57.14
Nahanni, Canada		0.0102	0.0880	0.0078	23.53
Imperial Valley-06		0.0032	0.0024	0.0018	43.75
Superstition Hills	FF	0.0049	0.0034	0.0021	57.14
Denali, Alaska		0.0079	0.0064	0.0051	35.44
San Fernando		0.0062	0.0032	0.0029	53.23
Irpinia, Italy-01		0.0072	0.0061	0.0048	33.33
Landers		0.0102	0.0094	0.0071	30.39
Manjil, Iran		0.0059	0.0042	0.0024	59.32
Nahanni, Canada		0.0152	0.0128	0.0102	32.89
Erzican, Turkey		0.0062	0.0048	0.0022	64.52
Chi-Chi, Taiwan		0.0125	0.0114	0.0102	18.40
Chi-Chi, Taiwan		0.0045	0.0034	0.0022	51.11



(a)



(b)

Fig. 14. Spectral response of NF and FF ground motions (5% damping).

Accordingly, this study investigates the vibration mitigation capabilities of NNBI under both vertical and horizontal components of near-field earthquake excitations. The seismic response of the NNBI-isolated TDOF system, obtained using the hybrid optimization technique and the concise analytical solutions, is illustrated in Fig. 15. Both methods successfully predict the optimal nonlinear response of the structure when regulated by the tuned NNBI parameters.

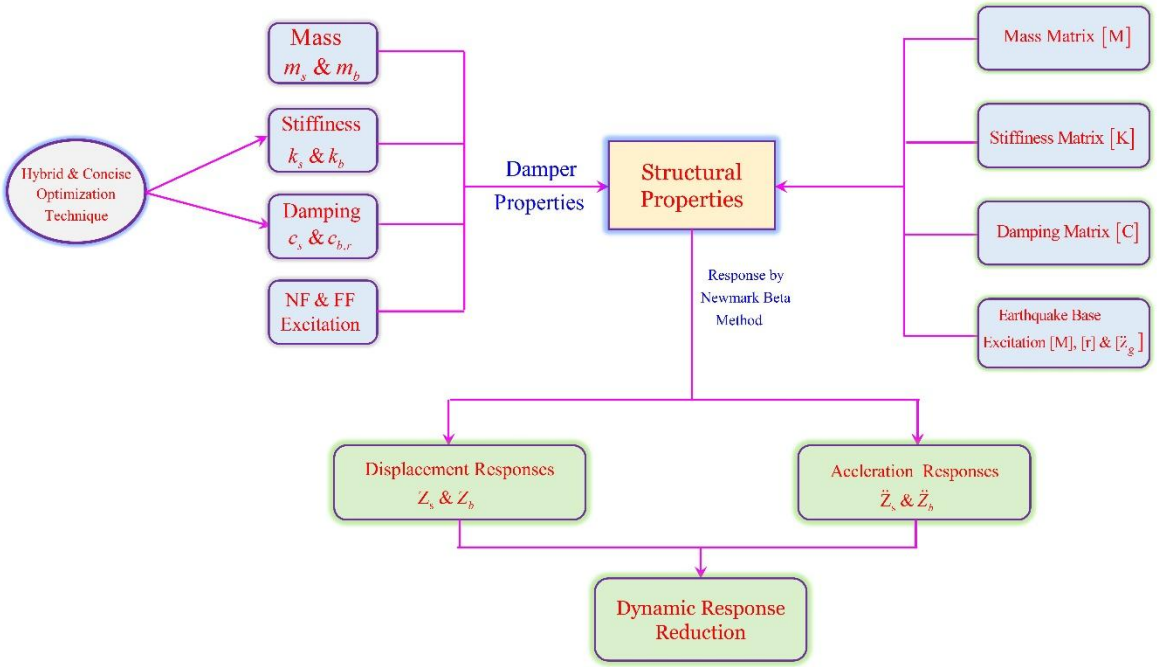
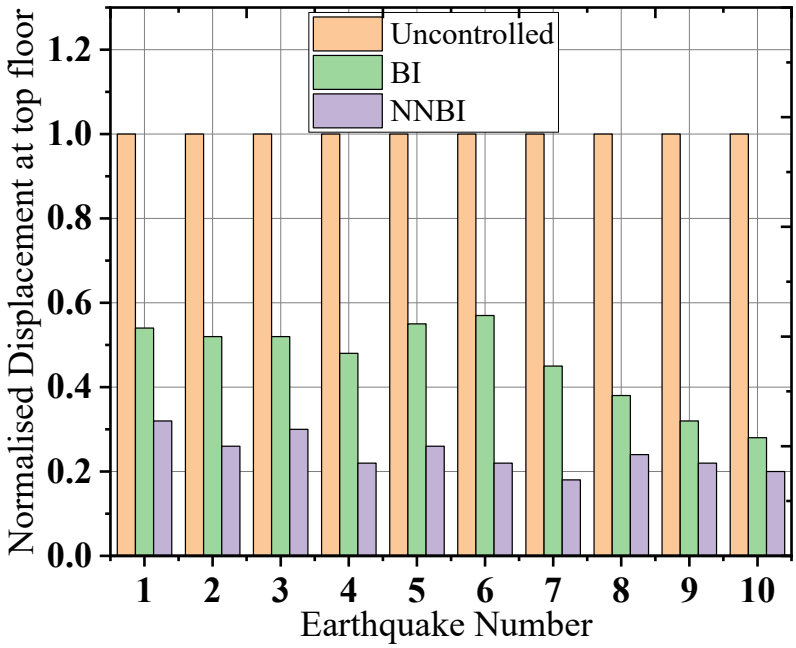
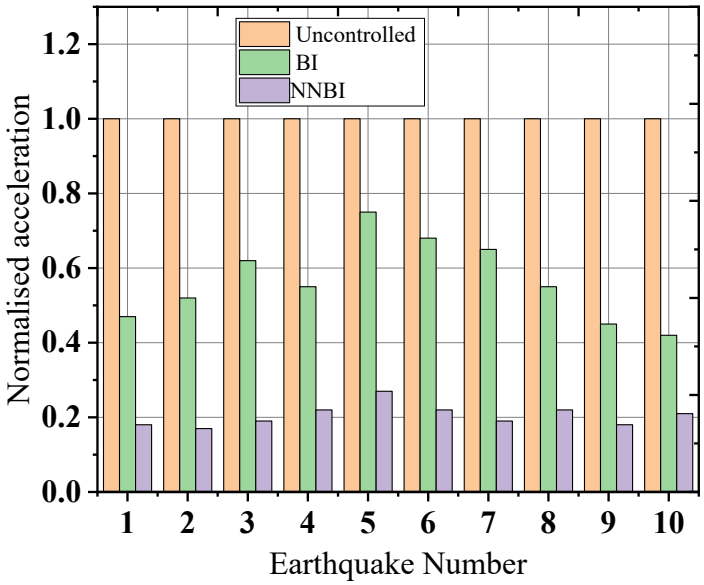


Fig. 15. Time-history response of NNBI-isolated system.

Fig. 16 compares the response of the TDOF system under all twenty earthquake records, with and without control devices. It is observed that both the conventional base isolator (BI) and the NNBI substantially mitigate seismic response across all excitations. However, theNNBI consistently provides superior vibration reduction, particularly for near-field motions characterized by forward-directivity pulses.



(b)



(b)

Fig. 16. Normalized response mitigation under 20 ground motions.

6.2 Stochastic Excitation Analysis using Clough–Penzien Spectrum

To complement the time-history analyses, the behavior of the model under stochastic excitation is also investigated. Here, a white noise excitation is considered, and the corresponding ground motion spectrum is modeled using the Clough–Penzien power spectral density function, which is based on a revised Kanai–Tajimi filter:

$$X_{\ddot{z}_g} = S_0 \frac{\omega_k^4 + 4\varsigma_k^2\omega_k^2\omega^2}{\left(\omega_k^2 - \omega^2\right)^2 + 4\varsigma_k^2\omega_k^2\omega^2} \times \frac{\omega^4}{\left(\omega_g^2 - \omega^2\right)^2 + 4\varsigma_g^2\omega_g^2\omega^2} \tag{64}$$

Where

- S_0 is the constant power spectral density of the white noise excitation,
- ω_k and ς_k are the natural frequency and damping ratio of the soil layer,
- ω_g and ς_g are the second filter parameters representing very low-frequency ground effects.

In this study, firm soil conditions are assumed, and filter parameters are selected from Ref. Kiureghian and Neuenhofer (1992).

Figure 17 illustrates the stochastic behaviour of the TDOF base-isolated system when subjected to white noise excitation. For the hybrid optimization technique, the highest spectral response values of the base-isolated structure are observed to be $2.9085 \times 10^5 dB/Hz$ for the BI and $1.8075 \times 10^5 dB/Hz$ for the NNBI, indicating a 36.84% improvement of the NNBI over the BI. Using the concise analytical solutions, the corresponding values are $1.7065 \times 10^5 dB/Hz$ (BI) and $6.5475 \times 10^5 dB/Hz$ (NNBI), showing that the NNBI achieves a 22.18% improvement in vibration mitigation compared to the BI.

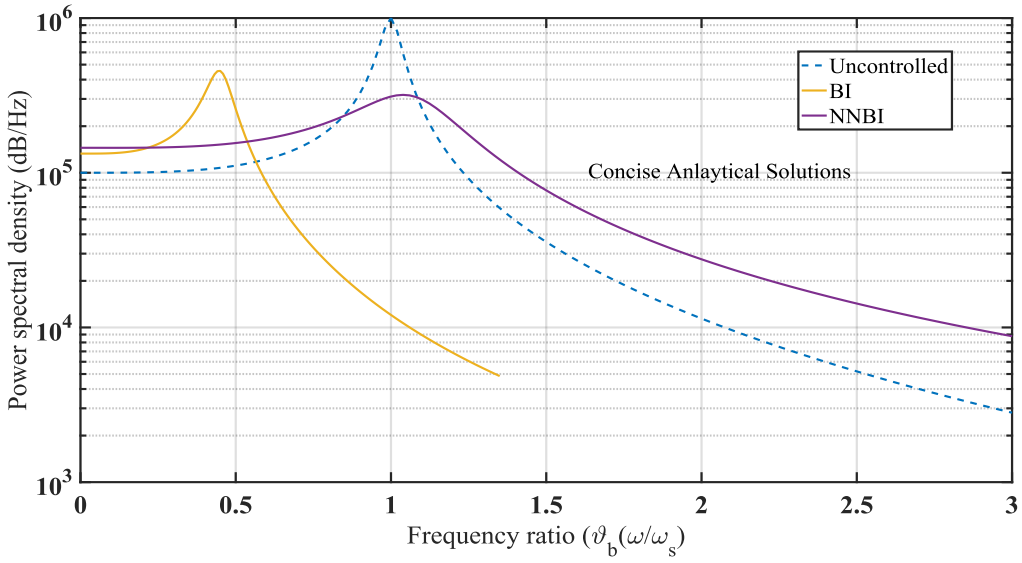


Fig. 17. Response mitigation under random white noise (Hybrid vs. Concise).

The results from both deterministic (time-history) and stochastic analyses highlight several key practical implications:

1. Design guidelines: The concise analytical solutions provide closed-form relationships that can be used by engineers to rapidly estimate isolator parameters without resorting to iterative optimization. This makes them suitable for preliminary seismic design of isolation systems, offering a balance between accuracy and computational simplicity.

2. Robustness under pulse-type excitations: The NNBI demonstrates clear advantages under near-field pulse-type motions, which are especially critical for isolated structures. The hybrid optimization framework ensures that the system remains effective under both horizontal and vertical components of severe near-field earthquakes.

3. Scalability to complex structures: While the present study focuses on an TDOF system, the methodology and closed-form solutions can be readily extended to MDOF systems and real buildings, where higher-mode effects and soil–structure interaction become significant. This enhances the practical relevance of the proposed NNBI framework for real-world seismic protection.

7. NUMERICAL MODEL VERIFICATION

In the present investigation, the proposed model with an integrated nonlinear negative stiffness damper subjected to bidirectional seismic excitations is analyzed. To ensure reliability, the results are benchmarked against previously published studies. The optimal isolator frequency ratio obtained in this work is compared with the model reported by Chowdhury et al., (2024), and the comparison is illustrated in Fig. 18. Similarly, the optimal damping ratio derived through the hybrid optimization technique is compared with the findings of Su, et al. (2024), illustrated in Fig. 19. Furthermore, the optimal damping ratio determined using the concise analytical solutions is compared with the results of Su et al. (2024), as presented in Fig. 20.

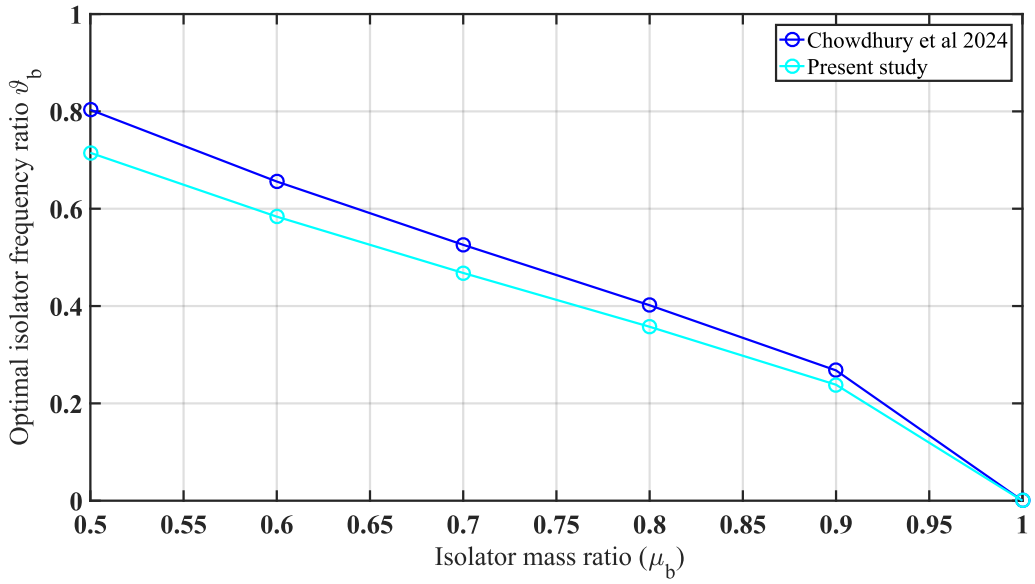


Fig. 18. Optimum frequency ratio: present study vs. Chowdhury et al. (2024).

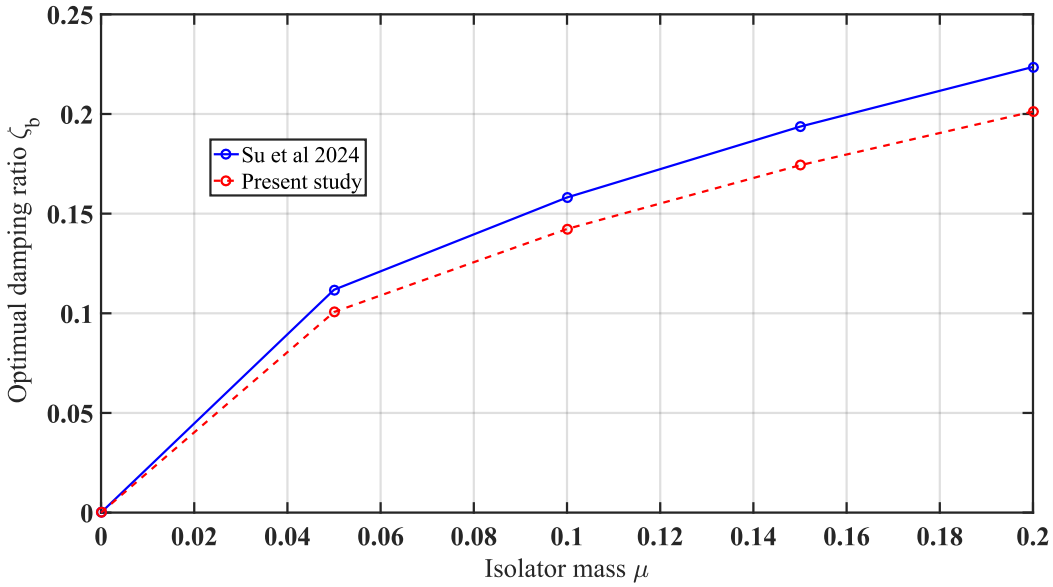


Fig. 19. Optimum damping ratio: present study vs. Su et al. (2024).

Overall, the comparisons show close consistency between the developed model and prior studies, confirming both the reliability and effectiveness of the proposed optimization schemes. The alignment of results across different methodologies and references reinforces the reliability of both the hybrid optimization technique and the concise analytical solutions for analyzing nonlinear isolator systems.

Beyond validating the model against prior studies, this work extends the current state of knowledge by explicitly bridging hybrid optimization with concise analytical formulations to capture nonlinear isolation effects under diverse excitations. The integration of near-field pulse-type motions, stochastic excitation modeling, and bidirectional seismic inputs demonstrates the robustness and generality of the proposed NNBI-based approach. These contributions not only refine the theoretical understanding of nonlinear base isolation but also provide a transferable framework for practical seismic design of isolated structures.

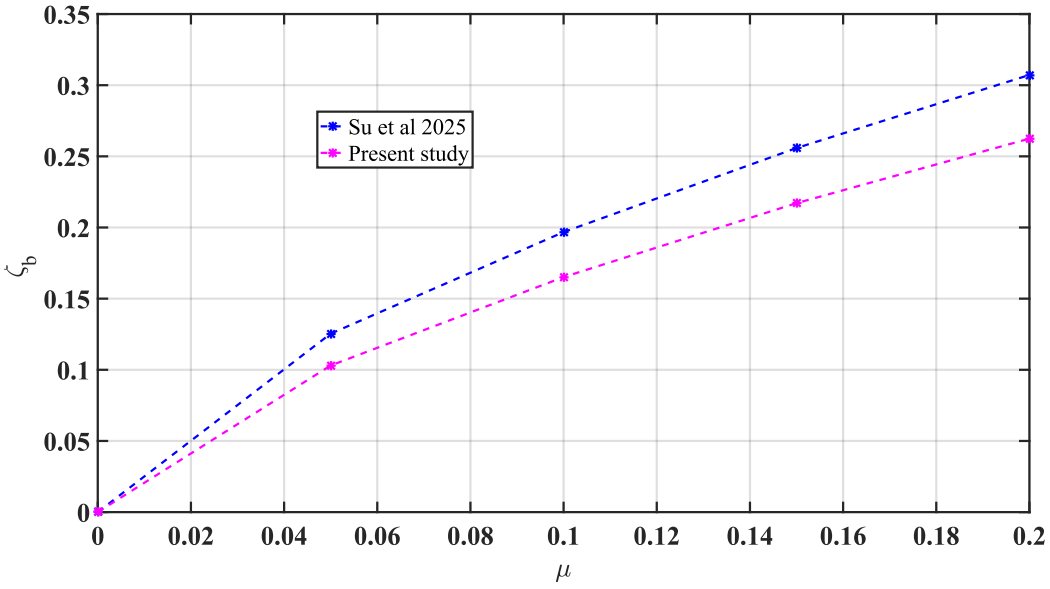


Fig. 20. Optimum damping ratio: present study vs. Su et al. (2025).

CONCLUSIONS

This study investigated the nonlinear dynamic behaviour of vibration isolation systems incorporating nonlinear negative stiffness elements under bidirectional excitation using both hybrid optimization and closed-form analytical approaches. The proposed framework, based on statistical linearization and analytical modelling, enabled the derivation of explicit expressions for optimal system parameters, providing an efficient alternative to conventional iterative optimization techniques.

The results demonstrate that the inclusion of negative stiffness significantly enhances vibration mitigation by effectively modifying the dynamic characteristics of the system, including resonance behaviour and energy distribution. In particular, the proposed system achieved response reductions exceeding 60% under representative excitation conditions, while improvements of approximately 20–40% were consistently observed under stochastic excitations. These findings confirm the robustness of the negative stiffness mechanism in reducing dynamic response amplitudes across different excitation types.

The closed-form analytical solutions provide rapid and transparent prediction of system response, making them well suited for preliminary design and parametric analysis, whereas the hybrid optimization approach enables refined parameter tuning for improved performance. Although the analytical solutions yield slightly conservative estimates compared to hybrid optimization, they offer greater physical insight into system behaviour.

Comparisons with existing studies confirm the validity and robustness of the proposed formulations, with close agreement observed in optimal frequency and damping parameters. Overall, the study establishes the potential of negative stiffness mechanisms as an effective strategy for vibration control in nonlinear dynamical systems. Future work will focus on extending the formulation to multi-degree-of-freedom systems and more complex loading scenarios to enhance its applicability to practical engineering systems.

REFERENCES

Akbari M, Zamani A-A, Seifi M, Pantò B, Falborski T, Jankowski R (2025) An optimal nonlinear fractional order controller for passive/active base isolation building equipped with friction-tuned mass dampers.

Communications in Nonlinear Science and Numerical Simulation 140:108405. https://doi.org/10.1016/j.cnsns.2024.108405

Al-Fahdawi OAS, Barroso LR (2021) Adaptive neuro-fuzzy and simple adaptive control methods for full three-dimensional coupled buildings subjected to bi-directional seismic excitations. Engineering Structures 232:111798. https://doi.org/10.1016/j.engstruct.2020.111798

Asami T, Nishihara O (1999) Analytical and Experimental Evaluation of an Air Damped Dynamic Vibration Absorber: Design Optimizations of the Three-Element Type Model. Journal of Vibration and Acoustics 121:334–342. https://doi.org/10.1115/1.2893985

Asami T, Nishihara O (2002) H2 Optimization of the Three-Element Type Dynamic Vibration Absorbers. Journal of Vibration and Acoustics 124:583–592. https://doi.org/10.1115/1.1501286

Asami T, Nishihara O, Baz AM (2002) Analytical Solutions to H∞ and H2 Optimization of Dynamic Vibration Absorbers Attached to Damped Linear Systems. Journal of Vibration and Acoustics 124:284–295. https://doi.org/10.1115/1.1456458

Bishop RED (1957) Mechanical Vibrations. Nature 179:504–504. https://doi.org/10.1038/179504a0

Carrella A, Brennan MJ, Kovacic I, Waters TP (2009) On the force transmissibility of a vibration isolator with quasi-zero-stiffness. Journal of Sound and Vibration 322:707–717. https://doi.org/10.1016/j.jsv.2008.11.034

Cheung YL, Wong WO (2011) H2 optimization of a non-traditional dynamic vibration absorber for vibration control of structures under random force excitation. Journal of Sound and Vibration 330:1039–1044. https://doi.org/10.1016/j.jsv.2010.10.031

Chowdhury S, Banerjee A (2023) The nonlinear dynamic analysis of optimum nonlinear inertial amplifier base isolators for vibration isolation. Nonlinear Dyn 111:12749–12786. https://doi.org/10.1007/s11071-023-08599-0

Chowdhury S, Banerjee A, Adhikari S (2022) Optimal negative stiffness inertial-amplifier-base-isolators: Exact closed-form expressions. International Journal of Mechanical Sciences 218:107044. https://doi.org/10.1016/j.ijmecsci.2021.107044

Chowdhury S, Banerjee A, Adhikari S (2024) Enhancing seismic resilience of structures through optimally designed nonlinear negative stiffness base isolators: Exact closed-form expressions. Nonlinear Dyn 112:15833–15856. https://doi.org/10.1007/s11071-024-09892-2

Colwell S, Basu B (2009) Tuned liquid column dampers in offshore wind turbines for structural control. Engineering Structures 31:358–368. https://doi.org/10.1016/j.engstruct.2008.09.001

De Luca A, Guidi LG (2019) State of art in the worldwide evolution of base isolation design. Soil Dynamics and Earthquake Engineering 125:105722. https://doi.org/10.1016/j.soildyn.2019.105722

Den Hartog J (1947) The Undamped and Damped Dynamic Vibration Absorbers. Mechanical Vibrations 3:112–113

Di Matteo A, Masnata C, Pirrotta A (2019) Simplified analytical solution for the optimal design of Tuned Mass Damper Inerter for base isolated structures. Mechanical Systems and Signal Processing 134:106337. https://doi.org/10.1016/j.ymssp.2019.106337

Efafi M, Hosseini SAA, Tourajizadeh H (2022) Robust Control and Vibration Reduction of a 3D Nonlinear Flexible Robotic Arm. Iran J Sci Technol Trans Mech Eng 46:1157–1173. https://doi.org/10.1007/s40997-021-00484-8

Garrido H, Curadelli O, Ambrosini D (2013) Improvement of tuned mass damper by using rotational inertia through tuned viscous mass damper. Engineering Structures 56:2149–2153. https://doi.org/10.1016/j.engstruct.2013.08.044

Hewage TAM, Alderson KL, Alderson A, Scarpa F (2016) Double-Negative Mechanical Metamaterials Displaying Simultaneous Negative Stiffness and Negative Poisson's Ratio Properties. 28:10323–10332. https://doi.org/10.1002/adma.201603959

Hosseinzadeh S, Galal K (2021) Probabilistic seismic resilience quantification of a reinforced masonry shear wall system with boundary elements under bi-directional horizontal excitations. Engineering Structures 247:113023. https://doi.org/10.1016/j.engstruct.2021.113023

Hu X, Zhou C (2025) A stable horizontal 3-DOF vibration isolation system with adjustable stiffness: Theoretical analysis and experiment. Mechanical Systems and Signal Processing 230:112631. https://doi.org/10.1016/j.ymssp.2025.112631

Hu Y, Chen MZQ (2015) Performance evaluation for inerter-based dynamic vibration absorbers. International Journal of Mechanical Sciences 99:297–307. https://doi.org/10.1016/j.ijmecsci.2015.06.003

Ikago K, Saito K, Inoue N (2012) Seismic control of single-degree-of-freedom structure using tuned viscous mass damper. Earthquake Engineering & Structural Dynamics 41:453–474. https://doi.org/10.1002/eqe.1138

Islam NU, Jangid RS (2023) Optimum parameters and performance of negative stiffness and inerter based dampers for base-isolated structures. Bull Earthquake Eng 21:1411–1438. https://doi.org/10.1007/s10518-022-01372-5

Jangid RS (2022a) Performance and optimal design of base-isolated structures with clutching inerter damper. Structural Control and Health Monitoring 29:e3000. https://doi.org/10.1002/stc.3000

Jangid RS (2022b) Seismic Performance Assessment of Clutching Inerter Damper for Isolated Bridges. Practice Periodical on Structural Design and Construction 27. https://doi.org/10.1061/(ASCE)SC.1943-5576.0000661

Jangid RS (2023) Seismic performance of a clutched inerter for structures with curved surface sliders. Structures 49:44–57. https://doi.org/10.1016/j.istruc.2023.01.057

Kapasakalis KA, Antoniadis IA, Sapountzakis EJ (2020) Performance assessment of the KDamper as a seismic Absorption Base. Structural Control and Health Monitoring 27:e2482. https://doi.org/10.1002/stc.2482

Kiran KK, Ahmad S, Al-Osta MA, Bahraq AA (2023) Enhancing the seismic resilience of structures by using optimum combination of tuned mass damper inerter and negative stiffness damper. Structures 57:105253. https://doi.org/10.1016/j.istruc.2023.105253

Kiran KK, Al-Osta MA, Ahmad S, Bahraq AA (2024) Optimal Design of Tuned Mass and Negative Stiffness Amplifier Dampers with Inerter by H2 Optimal Control Under Bidirectional Seismic Load. Arab J Sci Eng. https://doi.org/10.1007/s13369-024-08960-4

Kiran KK, Naveenkumar DT, Kumar AM (2025) Seismic vulnerability mitigation of base isolated structures equipped using a novel tuned mass dampers with H2 optimization. Asian J Civ Eng 26:1129–1142. https://doi.org/10.1007/s42107-024-01238-y

Kiureghian AD, Neuenhofer A (1992) Response spectrum method for multi-support seismic excitations. Earthquake Engineering & Structural Dynamics 21:713–740. https://doi.org/10.1002/eqe.4290210805

Li X, Zhao P, Jing X (2025) X-Stewart mechanism for vibration isolation with nonlinear translational-to-rotational motion properties. International Journal of Mechanical Sciences 303:110596. https://doi.org/10.1016/j.ijmecsci.2025.110596

Liu H, Huang X, Jiang Z, Li S, Rong Z (2024) Reliability-based design optimization scheme of isolation capacity of nonlinear vibration isolators. Engineering Structures 300:117220. https://doi.org/10.1016/j.engstruct.2023.117220

Lyu Q, Zhang Z, Fu B, Ye J, Liu L (2025) Seismic mitigation mechanism and optimal parameter analysis of tuned negative stiffness amplifying damper (TNSAD) for base-isolated structures. Journal of Building Engineering 111:113568. https://doi.org/10.1016/j.jobe.2025.113568

Matsagar VA, Jangid RS (2003) Seismic response of base-isolated structures during impact with adjacent structures. Engineering Structures 25:1311–1323. https://doi.org/10.1016/S0141-0296(03)00081-6

Niu M-Q, Zhuang Y-S, Han W-J, Chen L-Q (2024) History dependent analysis of compliant beams for nonlinear vibration isolation. International Journal of Mechanical Sciences 281:109571. https://doi.org/10.1016/j.ijmecsci.2024.109571

Ormondroyd J, Den Hartog JP (2023) The Theory of the Dynamic Vibration Absorber. Transactions of the American Society of Mechanical Engineers 49–50. https://doi.org/10.1115/1.4058553

Panchal VR, Jangid RS (2012) Behaviour of liquid storage tanks with VCFPS under near-fault ground motions. Structure and Infrastructure Engineering 8:71–88. https://doi.org/10.1080/15732470903300919

Pasala DTR, Sarlis AA, Nagarajaiah S, Reinhorn AM, Constantinou MC, Taylor D (2013) Adaptive Negative Stiffness: New Structural Modification Approach for Seismic Protection. Journal of Structural Engineering 139:1112–1123. https://doi.org/10.1061/(ASCE)ST.1943-541X.0000615

Rong K, Gong J, Tian L, Luo J, Li N (2025) Study on wind-induced vibration control and life-prolonging of large-span transmission tower-line system using bidirectional gas-spring damper. Advances in Structural Engineering 13694332251359327. https://doi.org/10.1177/13694332251359327

Roy-Layinde TO, Omoteso KA, Laoye JA, Diala UH (2025) Vibrational resonance in nonlinear vibration isolation systems. Mechanics Research Communications 148:104470. https://doi.org/10.1016/j.mechrescom.2025.104470

Shen Y, Peng H, Li X, Yang S (2017) Analytically optimal parameters of dynamic vibration absorber with negative stiffness. Mechanical Systems and Signal Processing 85:193–203. https://doi.org/10.1016/j.ymssp.2016.08.018

Shi Z, Cheng Z, Xiang H (2014) Seismic isolation foundations with effective attenuation zones. Soil Dynamics and Earthquake Engineering 57:143–151. https://doi.org/10.1016/j.soildyn.2013.11.009

Su N, Bian J, Chen Z, Xia Y (2023) A novel lever-type inerter-based vibration absorber. International Journal of Mechanical Sciences 254:108440. https://doi.org/10.1016/j.ijmecsci.2023.108440

Su N, Bian J, Peng S, Xia Y (2022a) Generic optimal design approach for inerter-based tuned mass systems. International Journal of Mechanical Sciences 233:107654. https://doi.org/10.1016/j.ijmecsci.2022.107654

Su N, Chen Z, Xia Y, Bian J (2024a) Hybrid analytical H-norm optimization approach for dynamic vibration absorbers. International Journal of Mechanical Sciences 264:108796. https://doi.org/10.1016/j.ijmecsci.2023.108796

Su N, Chen Z, Zeng C, Xia Y, Bian J (2024b) Concise analytical solutions to negative-stiffness inerter-based DVAs for seismic and wind hazards considering multi-target responses. Earthquake Engineering & Structural Dynamics 53:3820–3858. https://doi.org/10.1002/eqe.4199

Su N, Peng S, Hong N, Xia Y (2022b) Wind-induced vibration absorption using inerter-based double tuned mass dampers on slender structures. Journal of Building Engineering 58:104993. https://doi.org/10.1016/j.jobe.2022.104993

Su P, Jun C, Liu S, Wu J (2022c) Design and Analysis of a Vibration Isolator with Adjustable High Static–Low Dynamic Stiffness. Iran J Sci Technol Trans Mech Eng 46:1195–1207. https://doi.org/10.1007/s40997-022-00491-3

Tang Z, Luo H, Ikago K, Weng S, Zhu H (2025) Analytical optimization of rate-independent negative stiffness dampers for vibration control. International Journal of Mechanical Sciences 302:110548. https://doi.org/10.1016/j.ijmecsci.2025.110548

Wu J-C, Shih M-H, Lin Y-Y, Shen Y-C (2005) Design guidelines for tuned liquid column damper for structures responding to wind. Engineering Structures 27:1893–1905. https://doi.org/10.1016/j.engstruct.2005.05.009

Xiaoran W, Yongjun S, Shaopu Y (2016) H∞ optimization of the grounded three-element type dynamic vibration absorber. Journal of Dynamics &Control 14:448–453. https://doi.org/10.6052/1672-6553-2015-82

Xu T, Li Y, Lai T, Li S (2022) H2 and H∞ optimal designs of tuned inerter dampers for base motion excited structures with inherent damping. Journal of Vibration and Control. https://doi.org/10.1177/10775463221102254

Yan G, Lu J-J, Qi W-H, Zhao T-Y, Yan H, Zhao L-C, et al. (2023) Tetrahedron structure with nonlinear stiffness and inertia modulation for enhanced low frequency vibration isolation. Journal of Sound and Vibration 564:117897. https://doi.org/10.1016/j.jsv.2023.117897

Zhang L, Zhang R, Xie L, Xue S (2023) Dynamics and isolation performance of a vibration isolator with a yoke-type nonlinear inerter. International Journal of Mechanical Sciences 254:108447. https://doi.org/10.1016/j.ijmecsci.2023.108447

Zhang Y, Sun X, Xu J (2025) Isolation performances of combined system with large amplitude nonlinearity and dynamic vibration absorber. International Journal of Non-Linear Mechanics 105243. https://doi.org/10.1016/j.ijnonlinmec.2025.105243

Zhu L, Li X, Xiao H, Zhang C (2025) Numerical investigations on a novel resilient energy dissipation damper for multi-level earthquakes. Advances in Structural Engineering 13694332251363358. https://doi.org/10.1177/13694332251363358

Appendix A. Closed-Form Expressions for Eq. (20) and Eq. (22)

The coefficients $S_0 - S_4$ used in Eqs. (20) and (22) are expressed as follows:

$$S_0 = \frac{\mu_b^2\omega_s^2+\mu_b^4\omega_s^2\varsigma_b}{2(\alpha\kappa-1)} \tag{A1}$$

$$S_1 = \frac{\mu_b^2\omega_s^2\varsigma_s\nu_b+\mu_b^4\omega_s^2\varsigma_b}{2(\alpha\kappa-1)^3} \tag{A2}$$

$$S_2 = \frac{\mu_b^3\omega_s^3\varsigma_s\nu_b\nu^3+\mu_b^4\omega_s^2\varsigma_b}{2(\alpha\kappa-1)^2} \tag{A3}$$

$$S_3 = \frac{\mu_b^2\omega_s^2\varsigma_s\nu_b\nu^3\varsigma_b+\mu_b^4\omega_s^2\varsigma_b}{2(\alpha\kappa-1)^2} \tag{A4}$$

$$S_4 = \frac{\mu_b\omega_s\varsigma_s\nu_b\nu^3\varsigma_b+\mu_b^4\omega_s^2\varsigma_b}{2(\alpha\kappa-1)^3} \tag{A5}$$

Appendix B. Closed-Form Expressions for Eq. (35) and Eq. (37)

The coefficients $S_5 - S_8$ used in Eqs. (20) and (22) are expressed as follows:

$$S_5 = \frac{\mu_b^2\omega_s^2+\mu_b^4\omega_s^2\varsigma_b}{2(\alpha^2\kappa^2-1)} \tag{B6}$$

$$S_6 = \frac{\mu_b^2\omega_s^2\varsigma_s\nu_b+\mu_b^4\omega_s^2\varsigma_b}{2(\alpha^2\kappa^2-1)^3} \tag{B7}$$

$$S_7 = \frac{\mu_b^3\omega_s^3\varsigma_s\nu_b\nu^3+\mu_b^4\omega_s^2\varsigma_b}{2(\alpha^2\kappa^2-1)^2} \tag{B8}$$

$$S_8 = \frac{\mu_b^2\omega_s^2\varsigma_s\nu_b\nu^3\varsigma_b+\mu_b^4\omega_s^2\varsigma_b}{2(\alpha^2\kappa^2-1)^2} \tag{B9}$$

Appendix C. Ground Motions Considered in the Present Investigation

Table C.1. NF ground motion records used in the present study

Earthquake No.	Record Station No	Earthquake	Year	Magnitude	PGA (m/s^2)	PGV (m/s)
1	1504	Chi-Chi, Taiwan	1999	7.6	5.49	0.92
2	1176	Kocaeli, Turkey	1999	7.5	3.04	0.73
3	960	Northridge-01	1994	6.7	5.10	0.63
4	1116	Kobe, Japan	1995	6.9	5.00	0.37
5	1602	Duzce, Turkey	1999	7.1	8.04	0.62
6	825	Cape Mendocino	1992	7.0	14.01	1.20
7	802	Lama Prieta	1989	6.9	3.92	0.56
8	126	Gazli, USSR	1976	6.8	6.96	0.71
9	495	Nahanni, Canada	1985	7.0	7.15	0.70
10	160	Imperial Valley-06	1979	6.5	7.45	0.44

Table C.2. FF ground motion records used in the present study

Earthquake No.	Record Station No	Earthquake	Year	Magnitude	PGA (m/s^2)	PGV (m/s)
11	721	Superstition Hills	1987	6.5	3.53	0.46
12	2114	Denali, Alaska	2002	7.9	3.23	1.26
13	68	San Fernando	1971	6.6	2.06	0.19
14	292	Irpinia, Italy-01	1980	6.9	3.92	0.56
15	900	Landers	1992	7.3	2.35	0.52
16	1633	Manjil, Iran	1990	7.4	5.00	0.54
17	496	Nahanni, Canada	1985	6.8	4.41	0.35
18	821	Erzican, Turkey	1992	6.7	4.9	0.96
19	1529	Chi-Chi, Taiwan	1999	7.6	2.94	1.07
20	1503	Chi-Chi, Taiwan	1999	7.6	7.84	1.28

Appendix D. Closed Form Expression for Eq. (53)

$$A = \frac{11E_1^6\alpha^4\varepsilon^4\mu_b^4v_b^6}{v^{12}} \text{ and}$$
$$E_1 = (v^4 + 4v^2\varsigma_s^2 - 4v^2 + 2) \tag{D1}$$

$$B = -\frac{36E_1\alpha\varepsilon\mu_b^2v_b^2}{v^6} + \frac{36E_1^3\alpha\varepsilon\mu_b^2v_b^2}{v^8} - \frac{36E_1^3\alpha^2\kappa\mu_b^2v_b^4}{v^8} + \frac{36E_1^2\alpha\varepsilon\mu_bv_b^2}{v^4} - \frac{36E_1^2\alpha\varepsilon\mu_bv_b^2}{v^6} - \frac{118E_1^2\alpha\varepsilon\mu_bv_b^2\varsigma_s^2}{v^4} \tag{D2}$$

$$C = \begin{pmatrix} (32v^4 + 108v^2\varsigma_s^2 - 64v^2 + 32)\mu_b^2v_b^4v^4\alpha^2\kappa^2 + 8\mu_b^2v_b^4v^4\alpha^2\kappa^2\varsigma_s^2 \\ -4\mu_b^2v_b^2v^4\alpha^2\kappa^2 + 4\mu_b^2\alpha\kappa v_b^2v^6 - 4\mu_b^2\alpha\kappa v_b^4v^4 + 10\mu_b^2\alpha\kappa v_b^4v^4\varsigma_s^2 \\ -10\mu_b^2\alpha\kappa v_b^4v^2\varsigma_s^2 + 6\mu_b^2v_b^2\varsigma_b^2v^6 + 18\mu_b^2v_b^2\varsigma_b^2v^4\varsigma_s^2 + 10v^4\alpha\kappa\mu_bv_b^2\varsigma_s^2 \\ +\mu_b^2v_b^4\alpha^2\kappa^2 - 4\mu_b^2\alpha\kappa v_b^2v^4 + 6\mu_b^2\alpha\kappa v_b^4v^2 + \mu_b^2v^8 - 2\mu_b^2v^6v_b^2 \\ +4\mu_b^2v^6\varsigma_s^2 + \mu_b^2v^4v_b^4 - 10\mu_b^2v_b^2\varsigma_b^2v^4 - 8\mu_b^2v_b^2\varsigma_s^2v^4 + 4\mu_b^2v_b^4v^2\varsigma_s^2 \\ +10\mu_bv^6v_b\varsigma_b\varsigma_s - 2v^4\alpha\kappa\mu_bv_b^2 + 8v^6\varsigma_s^2\mu_b - 8v^4\varsigma_s^2\mu_bv_b^2 + 2\mu_b^2\alpha\kappa v_b^2v^2 \\ -2\mu_b^2\alpha\kappa v_b^4 - 2\mu_b^2v_b^6 + 4\mu_b^2v^4v_b^2 - 2\mu_b^2v^2v_b^4 + 4\mu_b^2v_b^2\varsigma_b^2v^6 \end{pmatrix} \tag{D3}$$

$$D = -16E_1^2 \tag{D4}$$

Appendix E. Optimum parameters of Nonlinear Negative Stiffness base isolators with respect to Hybrid Optimization Technique

Table E.1. Optimum parameters of NNBI obtained from hybrid optimization based on relative displacement criterion

μ	$\xi = 0$(Undamped)		$\xi = 0.02$		$\xi = 0.05$		$\xi = 0.075$		$\xi = 0.1$	
	v_b	ς_b	v_b	ς_b	v_b	ς_b	v_b	ς_b	v_b	ς_b
0.005	0.4988	0.0455	0.5027	0.0461	0.5087	0.0468	0.5136	0.0473	0.5186	0.0479
0.010	0.4975	0.0642	0.5030	0.0649	0.5113	0.0659	0.5183	0.0666	0.5252	0.0673
0.020	0.4950	0.0904	0.5027	0.0914	0.5142	0.0926	0.5237	0.0935	0.5333	0.0944
0.030	0.4926	0.1102	0.5018	0.1114	0.5156	0.1128	0.5270	0.1138	0.5385	0.1147
0.040	0.4902	0.1266	0.5006	0.1280	0.5162	0.1296	0.5292	0.1306	0.5422	0.1315
0.050	0.4878	0.1409	0.4992	0.1424	0.5164	0.1441	0.5307	0.1452	0.5450	0.1460
0.060	0.4854	0.1536	0.4977	0.1552	0.5162	0.1570	0.5316	0.1581	0.5470	0.1589
0.070	0.4831	0.1651	0.4962	0.1669	0.5158	0.1688	0.5321	0.1699	0.5485	0.1706
0.080	0.4808	0.1757	0.4945	0.1776	0.5151	0.1796	0.5323	0.1806	0.5495	0.1813
0.090	0.4785	0.1855	0.4928	0.1875	0.5143	0.1896	0.5323	0.1906	0.5502	0.1912
0.100	0.4762	0.1946	0.4911	0.1968	0.5134	0.1989	0.5320	0.1999	0.5506	0.2005
0.125	0.4706	0.2152	0.4866	0.2176	0.5105	0.2198	0.5305	0.2208	0.5505	0.2212
0.150	0.4651	0.2331	0.4819	0.2359	0.5071	0.2382	0.5281	0.2391	0.5491	0.2393
0.200	0.4545	0.2635	0.4724	0.2668	0.4992	0.2694	0.5215	0.2702	0.5438	0.2700
0.250	0.4444	0.2887	0.4627	0.2925	0.4902	0.2954	0.5131	0.2960	0.5359	0.2955
0.300	0.4348	0.3101	0.4531	0.3145	0.4805	0.3176	0.5033	0.3182	0.5261	0.3173
0.350	0.4255	0.3287	0.4434	0.3337	0.4702	0.3371	0.4925	0.3376	0.5149	0.3364
0.400	0.4167	0.3450	0.4338	0.3507	0.4595	0.3545	0.4809	0.3549	0.5024	0.3534
0.450	0.4082	0.3596	0.4243	0.3659	0.4485	0.3701	0.4687	0.3705	0.4888	0.3687
0.500	0.4000	0.3727	0.4149	0.3797	0.4372	0.3843	0.4558	0.3847	0.4744	0.3827
0.600	0.3846	0.3953	0.3963	0.4037	0.4139	0.4093	0.4285	0.4099	0.4431	0.4076
0.700	0.3704	0.4142	0.3781	0.4242	0.3898	0.4310	0.3995	0.4318	0.4092	0.4293
0.800	0.3571	0.4303	0.3603	0.4420	0.3650	0.4501	0.3690	0.4513	0.3729	0.4487
0.900	0.3448	0.4443	0.3428	0.4577	0.3397	0.4672	0.3371	0.4690	0.3346	0.4664
1.000	0.3333	0.4564	0.3255	0.4717	0.3139	0.4828	0.3041	0.4853	0.2944	0.4829

Table E.2. Optimum parameters of NNBI obtained from hybrid optimization based on relative velocity criterion

μ	$\xi = 0$(Undamped)		$\xi = 0.02$		$\xi = 0.05$		$\xi = 0.075$		$\xi = 0.1$	
	υ_b	ς_b	υ_b	ς_b	υ_b	ς_b	υ_b	ς_b	υ_b	ς_b
0.005	0.9969	-4.3862	0.9973	-3.5717	0.9979	-3.5716	0.9984	-3.5716	0.9990	-3.5715
0.010	0.9938	-4.3826	0.9944	-3.5701	0.9952	-3.5700	0.9960	-3.5699	0.9967	-3.5698
0.020	0.9877	-4.3753	0.9885	-3.5669	0.9897	-3.5667	0.9907	-3.5665	0.9917	-3.5663
0.030	0.9817	-4.3681	0.9827	-3.5636	0.9841	-3.5633	0.9853	-3.5631	0.9865	-3.5627
0.040	0.9759	-4.3608	0.9769	-3.5602	0.9786	-3.5599	0.9799	-3.5595	0.9813	-3.5591
0.050	0.9701	-4.3535	0.9713	-3.5568	0.9730	-3.5564	0.9745	-3.5560	0.9760	-3.5554
0.060	0.9644	-4.3462	0.9657	-3.5533	0.9676	-3.5529	0.9692	-3.5523	0.9708	-3.5517
0.070	0.9588	-4.3389	0.9601	-3.5498	0.9622	-3.5492	0.9639	-3.5486	0.9656	-3.5479
0.080	0.9533	-4.3316	0.9547	-3.5462	0.9568	-3.5456	0.9586	-3.5448	0.9604	-3.5440
0.090	0.9479	-4.3242	0.9494	-3.5426	0.9516	-3.5418	0.9534	-3.5410	0.9552	-3.5401
0.100	0.9426	-4.3168	0.9441	-3.5388	0.9464	-3.5380	0.9483	-3.5371	0.9501	-3.5361
0.125	0.9296	-4.2983	0.9312	-3.5293	0.9336	-3.5283	0.9357	-3.5271	0.9377	-3.5258
0.150	0.9172	-4.2796	0.9188	-3.5193	0.9213	-3.5181	0.9234	-3.5168	0.9255	-3.5152
0.200	0.8937	-4.2419	0.8954	-3.4983	0.8979	-3.4967	0.9000	-3.4949	0.9022	-3.4928
0.250	0.8718	-4.2037	0.8734	-3.4759	0.8759	-3.4739	0.8780	-3.4716	0.8801	-3.4689
0.300	0.8514	-4.1650	0.8529	-3.4520	0.8553	-3.4496	0.8573	-3.4469	0.8592	-3.4437
0.350	0.8323	-4.1259	0.8337	-3.4268	0.8358	-3.4240	0.8376	-3.4208	0.8394	-3.4171
0.400	0.8144	-4.0863	0.8156	-3.4003	0.8174	-3.3970	0.8190	-3.3934	0.8205	-3.3891
0.450	0.7976	-4.0463	0.7986	-3.3725	0.8000	-3.3688	0.8013	-3.3648	0.8025	-3.3599
0.500	0.7817	-4.0059	0.7824	-3.3435	0.7835	-3.3394	0.7844	-3.3349	0.7852	-3.3295
0.600	0.7526	-3.9240	0.7527	-3.2820	0.7527	-3.2772	0.7528	-3.2717	0.7529	-3.2653
0.700	0.7264	-3.8407	0.7257	-3.2164	0.7247	-3.2107	0.7238	-3.2044	0.7229	-3.1969
0.800	0.7027	-3.7561	0.7012	-3.1469	0.6988	-3.1405	0.6968	-3.1333	0.6949	-3.1247
0.900	0.6812	-3.6703	0.6786	-3.0741	0.6748	-3.0668	0.6717	-3.0587	0.6685	-3.0490
1.000	0.6614	-3.5836	0.6579	-2.9982	0.6525	-2.9901	0.6480	-2.9810	0.6436	-2.9703

Table E.3. Optimum parameters of NNBI obtained from hybrid optimization based on relative acceleration criterion

μ	$\xi = 0$(Undamped)		$\xi = 0.02$		$\xi = 0.05$		$\xi = 0.075$		$\xi = 0.1$	
	v_b	ς_b	v_b	ς_b	v_b	ς_b	v_b	ς_b	v_b	ς_b
0.005	0.9832	-6.7800	0.9814	-6.7800	0.9788	-6.7800	0.9766	-6.7800	0.9743	-6.7800
0.010	0.9755	-6.7579	0.9731	-6.7579	0.9694	-6.7579	0.9664	-6.7578	0.9634	-6.7578
0.020	0.9639	-6.7228	0.9606	-6.7227	0.9557	-6.7227	0.9516	-6.7226	0.9475	-6.7225
0.030	0.9545	-6.6927	0.9506	-6.6927	0.9448	-6.6926	0.9399	-6.6925	0.9351	-6.6923
0.040	0.9461	-6.6654	0.9418	-6.6653	0.9353	-6.6652	0.9298	-6.6651	0.9244	-6.6648
0.050	0.9385	-6.6397	0.9338	-6.6397	0.9267	-6.6396	0.9207	-6.6394	0.9148	-6.6391
0.060	0.9314	-6.6153	0.9264	-6.6153	0.9187	-6.6151	0.9124	-6.6149	0.9060	-6.6145
0.070	0.9247	-6.5918	0.9194	-6.5918	0.9113	-6.5916	0.9046	-6.5913	0.8979	-6.5909
0.080	0.9184	-6.5690	0.9127	-6.5690	0.9043	-6.5688	0.8972	-6.5684	0.8902	-6.5680
0.090	0.9122	-6.5469	0.9064	-6.5468	0.8976	-6.5466	0.8902	-6.5462	0.8829	-6.5457
0.100	0.9063	-6.5252	0.9002	-6.5252	0.8911	-6.5249	0.8835	-6.5245	0.8759	-6.5239
0.125	0.8924	-6.4729	0.8858	-6.4729	0.8760	-6.4725	0.8679	-6.4720	0.8597	-6.4713
0.150	0.8793	-6.4226	0.8724	-6.4225	0.8620	-6.4221	0.8534	-6.4215	0.8447	-6.4206
0.200	0.8551	-6.3262	0.8476	-6.3261	0.8363	-6.3255	0.8269	-6.3247	0.8176	-6.3236
0.250	0.8328	-6.2338	0.8249	-6.2337	0.8129	-6.2330	0.8030	-6.2320	0.7930	-6.2305
0.300	0.8120	-6.1444	0.8037	-6.1442	0.7912	-6.1434	0.7808	-6.1422	0.7704	-6.1404
0.350	0.7924	-6.0571	0.7838	-6.0569	0.7708	-6.0560	0.7600	-6.0546	0.7493	-6.0526
0.400	0.7737	-5.9717	0.7648	-5.9715	0.7515	-5.9704	0.7404	-5.9687	0.7293	-5.9665
0.450	0.7559	-5.8877	0.7468	-5.8875	0.7331	-5.8862	0.7217	-5.8844	0.7103	-5.8818
0.500	0.7389	-5.8050	0.7295	-5.8047	0.7155	-5.8033	0.7039	-5.8013	0.6922	-5.7984
0.600	0.7066	-5.6425	0.6969	-5.6422	0.6823	-5.6406	0.6702	-5.6381	0.6580	-5.6347
0.700	0.6766	-5.4833	0.6665	-5.4830	0.6513	-5.4810	0.6387	-5.4782	0.6261	-5.4742
0.800	0.6484	-5.3267	0.6379	-5.3263	0.6222	-5.3241	0.6091	-5.3209	0.5960	-5.3163
0.900	0.6217	-5.1723	0.6109	-5.1718	0.5946	-5.1693	0.5810	-5.1656	0.5675	-5.1605
1.000	0.5965	-5.0196	0.5852	-5.0163	0.5683	-6.7800	0.5543	-6.7800	0.5402	-5.0065

Appendix F. Optimum Parameters of Nonlinear Negative Stiffness Base Isolators using Concise Analytical Solutions with Taylor Coefficients

Table F.1. Optimum parameters of NNBI obtained from concise analytical solutions based on relative displacement criterion

μ	$\xi = 0$(Undamped)		$\xi = 0.02$		$\xi = 0.05$		$\xi = 0.075$		$\xi = 0.1$	
	υ_b	ς_b	υ_b	ς_b	υ_b	ς_b	υ_b	ς_b	υ_b	ς_b
0.005	0.9950	0.0432	0.9915	0.0444	0.9862	0.0461	0.9819	0.0476	0.9775	0.0491
0.010	0.9901	0.0609	0.9851	0.0626	0.9776	0.0650	0.9714	0.0671	0.9651	0.0691
0.020	0.9804	0.0857	0.9733	0.0880	0.9626	0.0913	0.9538	0.0941	0.9449	0.0970
0.030	0.9709	0.1045	0.9622	0.1071	0.9491	0.1111	0.9382	0.1144	0.9273	0.1178
0.040	0.9615	0.1201	0.9515	0.1230	0.9364	0.1274	0.9239	0.1312	0.9113	0.1349
0.050	0.9524	0.1336	0.9412	0.1368	0.9243	0.1415	0.9103	0.1455	0.8963	0.1496
0.060	0.9434	0.1457	0.9311	0.1490	0.9128	0.1540	0.8975	0.1582	0.8821	0.1625
0.070	0.9346	0.1566	0.9214	0.1601	0.9016	0.1653	0.8851	0.1696	0.8686	0.1740
0.080	0.9259	0.1667	0.9119	0.1702	0.8908	0.1755	0.8733	0.1800	0.8557	0.1845
0.090	0.9174	0.1760	0.9026	0.1795	0.8804	0.1849	0.8618	0.1895	0.8433	0.1941
0.100	0.9091	0.1846	0.8935	0.1882	0.8702	0.1937	0.8508	0.1982	0.8313	0.2029
0.125	0.8889	0.2041	0.8717	0.2076	0.8460	0.2130	0.8245	0.2175	0.8031	0.2221
0.150	0.8696	0.2212	0.8510	0.2245	0.8233	0.2295	0.8001	0.2338	0.7770	0.2382
0.200	0.8333	0.2500	0.8127	0.2526	0.7816	0.2566	0.7558	0.2600	0.7300	0.2636
0.250	0.8000	0.2739	0.7777	0.2754	0.7444	0.2778	0.7166	0.2799	0.6887	0.2822
0.300	0.7692	0.2942	0.7459	0.2943	0.7108	0.2947	0.6816	0.2951	0.6523	0.2958
0.350	0.7407	0.3118	0.7166	0.3103	0.6804	0.3082	0.6503	0.3067	0.6201	0.3054
0.400	0.7143	0.3273	0.6897	0.3240	0.6529	0.3191	0.6222	0.3154	0.5915	0.3118
0.450	0.6897	0.3411	0.6650	0.3357	0.6279	0.3278	0.5970	0.3215	0.5661	0.3154
0.500	0.6667	0.3536	0.6421	0.3459	0.6052	0.3346	0.5744	0.3255	0.5437	0.3167
0.600	0.6250	0.3750	0.6013	0.3623	0.5657	0.3435	0.5361	0.3282	0.5065	0.3133
0.700	0.5882	0.3930	0.5662	0.3745	0.5332	0.3474	0.5057	0.3251	0.4782	0.3032
0.800	0.5556	0.4082	0.5359	0.3836	0.5065	0.3471	0.4820	0.3172	0.4575	0.2876
0.900	0.5263	0.4215	0.5097	0.3900	0.4848	0.3435	0.4641	0.3051	0.4433	0.2673
1.000	0.5000	0.4330	0.4870	0.3943	0.4675	0.3369	0.4513	0.2896	0.4350	0.2429

Table F.2. Optimum parameters of NNBI obtained from concise analytical solutions based on relative velocity criterion

μ	$\xi = 0$(Undamped)		$\xi = 0.02$		$\xi = 0.05$		$\xi = 0.075$		$\xi = 0.1$	
	v_b	ς_b	v_b	ς_b	v_b	ς_b	v_b	ς_b	v_b	ς_b
0.005	1.6798	0.0082	1.6798	0.0095	1.6799	0.0114	1.6799	0.0131	1.6800	0.0147
0.010	1.6652	0.0115	1.6653	0.0133	1.6654	0.0160	1.6656	0.0183	1.6657	0.0206
0.020	1.6418	0.0163	1.6420	0.0187	1.6423	0.0224	1.6425	0.0254	1.6428	0.0285
0.030	1.6217	0.0200	1.6219	0.0228	1.6224	0.0270	1.6228	0.0305	1.6231	0.0341
0.040	1.6032	0.0231	1.6036	0.0261	1.6042	0.0307	1.6047	0.0345	1.6052	0.0385
0.050	1.5859	0.0258	1.5864	0.0290	1.5871	0.0338	1.5878	0.0378	1.5884	0.0420
0.060	1.5694	0.0283	1.5700	0.0315	1.5709	0.0364	1.5716	0.0406	1.5724	0.0448
0.070	1.5535	0.0305	1.5542	0.0338	1.5553	0.0387	1.5561	0.0429	1.5570	0.0472
0.080	1.5382	0.0327	1.5390	0.0358	1.5402	0.0407	1.5411	0.0448	1.5421	0.0491
0.090	1.5233	0.0346	1.5242	0.0377	1.5255	0.0424	1.5266	0.0465	1.5277	0.0506
0.100	1.5087	0.0365	1.5097	0.0394	1.5112	0.0439	1.5124	0.0479	1.5136	0.0519
0.125	1.4736	0.0408	1.4749	0.0432	1.4767	0.0470	1.4783	0.0503	1.4798	0.0538
0.150	1.4401	0.0447	1.4416	0.0464	1.4438	0.0491	1.4456	0.0517	1.4475	0.0543
0.200	1.3765	0.0516	1.3785	0.0513	1.3814	0.0513	1.3839	0.0516	1.3863	0.0521
0.250	1.3164	0.0576	1.3189	0.0549	1.3226	0.0513	1.3257	0.0486	1.3287	0.0462
0.300	1.2591	0.0630	1.2621	0.0575	1.2665	0.0495	1.2702	0.0433	1.2739	0.0374
0.350	1.2040	0.0680	1.2075	0.0591	1.2127	0.0462	1.2170	0.0360	1.2213	0.0262
0.400	1.1508	0.0726	1.1548	0.0600	1.1607	0.0417	1.1656	0.0270	1.1706	0.0127
0.450	1.0993	0.0769	1.1037	0.0603	1.1104	0.0360	1.1159	0.0164	1.1215	-0.0027
0.500	1.0492	0.0810	1.0541	0.0600	1.0615	0.0293	1.0676	0.0043	1.0738	-0.0200
0.600	0.9526	0.0885	0.9585	0.0579	0.9673	0.0130	0.9747	-0.0236	0.9821	-0.0595
0.700	0.8601	0.0952	0.8670	0.0541	0.8773	-0.0066	0.8859	-0.0562	0.8946	-0.1049
0.800	0.7710	0.1014	0.7789	0.0487	0.7907	-0.0291	0.8006	-0.0929	0.8104	-0.1557
0.900	0.6848	0.1072	0.6937	0.0420	0.7070	-0.0543	0.7181	-0.1334	0.7292	-0.2114
1.000	0.6011	0.1125	0.6110	0.0341	0.6257	-0.0820	0.6381	-0.1775	0.6504	-0.2716

Table F.3. Optimum parameters of NNBI obtained from concise analytical solutions based on relative acceleration criterion

μ	$\xi = 0$(Undamped)		$\xi = 0.02$		$\xi = 0.05$		$\xi = 0.075$		$\xi = 0.1$	
	υ_b	ς_b	υ_b	ς_b	υ_b	ς_b	υ_b	ς_b	υ_b	ς_b
0.005	0.9897	0.1316	0.9918	0.1338	0.9949	0.1371	0.9975	0.1398	1.0001	0.1426
0.010	0.9840	0.1854	0.9869	0.1884	0.9912	0.1930	0.9948	0.1969	0.9983	0.2007
0.020	0.9746	0.2604	0.9785	0.2645	0.9844	0.2708	0.9893	0.2760	0.9942	0.2813
0.030	0.9663	0.3169	0.9709	0.3218	0.9779	0.3291	0.9837	0.3353	0.9896	0.3415
0.040	0.9586	0.3638	0.9638	0.3691	0.9717	0.3772	0.9782	0.3841	0.9848	0.3910
0.050	0.9513	0.4043	0.9570	0.4100	0.9656	0.4187	0.9727	0.4260	0.9798	0.4334
0.060	0.9443	0.4404	0.9504	0.4464	0.9596	0.4554	0.9672	0.4630	0.9748	0.4708
0.070	0.9376	0.4731	0.9441	0.4791	0.9537	0.4884	0.9618	0.4963	0.9698	0.5042
0.080	0.9311	0.5029	0.9379	0.5091	0.9479	0.5185	0.9563	0.5264	0.9647	0.5346
0.090	0.9248	0.5306	0.9318	0.5367	0.9422	0.5461	0.9509	0.5541	0.9596	0.5623
0.100	0.9187	0.5563	0.9258	0.5623	0.9366	0.5717	0.9455	0.5796	0.9545	0.5878
0.125	0.9039	0.6139	0.9115	0.6195	0.9228	0.6283	0.9322	0.6359	0.9417	0.6437
0.150	0.8899	0.6640	0.8977	0.6690	0.9094	0.6768	0.9191	0.6836	0.9288	0.6907
0.200	0.8637	0.7482	0.8716	0.7511	0.8835	0.7560	0.8934	0.7604	0.9033	0.7652
0.250	0.8394	0.8172	0.8472	0.8173	0.8588	0.8181	0.8684	0.8192	0.8781	0.8208
0.300	0.8168	0.8753	0.8241	0.8720	0.8350	0.8678	0.8441	0.8648	0.8532	0.8624
0.350	0.7956	0.9253	0.8022	0.9180	0.8121	0.9079	0.8204	0.9001	0.8287	0.8929
0.400	0.7756	0.9688	0.7813	0.9570	0.7900	0.9403	0.7972	0.9271	0.8044	0.9146
0.450	0.7567	1.0071	0.7614	0.9904	0.7685	0.9663	0.7745	0.9471	0.7804	0.9287
0.500	0.7387	1.0411	0.7423	1.0191	0.7477	0.9870	0.7522	0.9613	0.7567	0.9365
0.600	0.7054	1.0988	0.7063	1.0649	0.7076	1.0153	0.7087	0.9751	0.7099	0.9360
0.700	0.6749	1.1459	0.6727	1.0987	0.6694	1.0293	0.6666	0.9729	0.6638	0.9177
0.800	0.6470	1.1848	0.6412	1.1230	0.6326	1.0321	0.6254	0.9579	0.6182	0.8851
0.900	0.6211	1.2174	0.6115	1.1399	0.5971	1.0256	0.5851	0.9321	0.5730	0.8401
1.000	0.5971	1.2449	0.5833	1.1506	0.5626	1.0112	0.5453	0.8971	0.5281	0.7847